Optimal Reactive Power Dispatch Based on Multi-strategy Improved Aquila Optimization Algorithm

Hongyu Long, Shanghua Liu, Tewei Chen, Hao Tan*, Jinzhu Wei, Chaohua Zhang, Wenchen Chen

***Abstract*—With the rapid development of artificial intelligence algorithms, using heuristic search optimization algorithms to solve optimal reactive power dispatch (ORPD) problem has become a hot topic for current research. ORPD is a multi-polar, non-convex and non-linear problem with a large number and type of constraints as well as discrete nature of control variables. This paper proposed a multi-strategy improved Aquila optimization (IAO) algorithm to solve the ORPD, which introduces a probabilistic perturbation strategy to improve the balance between global exploitation and local exploration, introduces a Cauchy operator to increase the population diversity of Aquila, introduces an elite group navigation strategy to further avoid falling into a local optimum, and analyzes the performance of IAO. To verify the validity of the proposed method in solving the ORPD problem, firstly, the simulation experiments of single-objective ORPD (SOORPD) are carried out on four test systems of different sizes, IEEE14-bus, IEEE30-bus, IEEE57-bus and IEEE118-bus, respectively. Then, to further verify the validity of the method, the simulation experiments of multi-objective ORPD (MOORPD) are carried out on the test system of IEEE30-bus with the method and other classical algorithms. Finally, Comparing the results of the proposed method, with the results of other classical optimization algorithms and the results of existing literature, the comparative analysis of the simulation results confirms the reliability and validity of the proposed method toward solving the ORPD problem.**

***Index Terms*—Multi-strategy; single-objective; intelligence algorithm; multi-objective**

Manuscript received July 2, 2022; revised November 5, 2022. This work was supported by the National Natural Science Foundation of China (51207064).

Hongyu Long is a professor level senior engineer at Chongqing Key Laboratory of Complex Systems and Bionic Control, Chongqing University of Posts and Telecommunications, Chongqing 400065, China (e-mail: longhongyu20@163.com).

Shanghua Liu is a postgraduate student at Chongqing Key Laboratory of Complex Systems and Bionic Control, Chongqing University of Posts and Telecommunications, Chongqing 400065, China (e-mail: liushanghua_cq@163.com).

Tewei Chen is a general manager of State Grid Chongqing Qianjiang Power Supply Company, Chongqing 409000, China (e-mail: chentewei_qj@163.com).

Hao Tan is a senior engineer at the Economic and Technology Research Institute, State Grid Chongqing Electric Power Company, Chongqing 401120, China (corresponding author to provide phone: +8613996108500; e-mail: tanhao_cq@163.com).

Jinzhu Wei is an engineer of State Grid Chongqing Qianjiang Power Supply Company, Chongqing 409000, China (e-mail: weijinzhu_qj@163.com).

Chaohua Zhang is a senior economist at the Economic and Technology Research Institute, State Grid Chongqing Electric Power Company, Chongqing 401120, China (e-mail: zhangchaohua_cq@163.com).

Wenchen Chen is an assistant engineer of State Grid Chongqing Qianjiang Power Supply Company, Chongqing 409000, China (e-mail: chenwenchen_qj@163.com).

I. Introduction

In past studies, optimal reactive power dispatch (ORPD) has played a vital role in modern power system planning as an effective way to improve power quality and enhance the safety and stability of grid operation. Therefore, it has received the attention of many researchers working in the power system industry. The ORPD problem is a complex optimization problem with both discrete and continuous variables, nonlinear inequality and equality constraints, and a nonlinear objective function. In theory, the ORPD is to adjust the reactive power flow by adjusting the generator terminal voltage, the reactive power output of reactive power compensation equipment and transformer tap ratio to finally find the most reasonable distribution of reactive power [1]. And the most rational distribution means regulating the reactive power at each branch in the system so that one or several indicators of the grid are optimized, while ensuring that the state variables are within the specified limits. More importantly, rational reactive power distribution has a direct impact on the voltage operating level [2]. Voltage, as an evaluation criterion for the power quality of the power system and an important indicator for safe and economic operation, is influenced by the reactive power distribution. For instance, the low voltage will lead to the failure of full-load output and thus affect the stability of the power system, while high voltage will lead to equipment damage and thus affect the power generation. Therefore, it is the eventual aim of the ORPD that the stability of system voltage is ensured, the network losses are reduced, and the safety, stability, and economy of the power system are improved [3-6].

As one of the branches of the optimal power flow, the ORPD is considered a nonlinear optimization problem. In the past, many traditional optimization methods are applied in solution of the ORPD, like quadratic interior point method [7], and mixed integer programming [8], etc. However, the traditional approaches require demanding conditions to solve the ORPD, such as the derivability of the objective function and the continuity of the variables. To address these drawbacks, many researchers have applied artificial intelligence algorithms to solve the ORPD. It does not require any properties of the variables and the objective function and can easily find the global optimal solution, which successfully compensates for the shortcomings of traditional optimization methods. In recent years, the intelligent optimization algorithms have been used to solve the ORPD including particle swarm algorithm (PSO) [9], beetle antennae search algorithm (BAS) [10], pigeon-inspired algorithm (PIO) [11], non-dominated sorting genetic

algorithm II (NSGA-II) [12], manta ray foraging optimization algorithm (MRFO) [13], artificial bee colony algorithm (ABC) [14], whale optimization algorithm (WOA) [15], imperialist competitive algorithm (ICA) [16], harmony search algorithm (HAS) [17], and gravitational search algorithm (GSA) [18], etc. However, these methods also suffer from the drawbacks of premature convergence, parameter dependence on random distribution and the tendency to fall into local optimum in solving complex high-dimensional ORPD problems [19]. Similarly, The Aquila optimization (AO) algorithm also suffers from insufficient population diversity and possibly dropping into a local optimum. In this paper, the proposed IAO and the classical algorithm are used to conduct power system SOORPD simulation experiments based on MATLAB software. The objective targets minimize active power loss (P_{loss}), minimize voltage deviation (V_d) and minimize voltage stability index (L_{index}) of the grid, respectively. And simulation systems include four test systems of different sizes, IEEE14-bus, IEEE30-bus, IEEE57-bus and IEEE118-bus. The results of the experiments showcase the validity of the improved strategy and the superiority of IAO. Moreover, in specific practical engineering applications, MOORPD is of great practical significance in solving real power system problems. Therefore, if any two of the three objective functions are simultaneously optimized, and simulation experiments of the MOORPD are conducted in a moderately sized IEEE 30-bus test system, the experimental results indicate the feasibility of the proposed method, and well-distributed Pareto fronts and better Pareto solutions can be obtained. This method was first applied to the ORPD.

The remaining framework of this paper is structured as follows. Section II gives the formulation definition of the ORPD and constraint handling strategy. Section III reviews the standard AO and proposes corresponding improve strategies for its shortcomings and analyzes the performance of IAO. Section IV describes how to apply IAO to the ORPD of power systems and analyzes and discusses its simulation results. Finally, Section V gives the conclusion.

II. Problem Formulation

The ORPD serves to optimize the operation of the power system to improve the reliability, economy and safety of the grid operation by adjusting the reactive power flow through the voltage at the generator terminals, the reactive power output of the reactive power compensation equipment and the transformer tap ratio.

The ORPD can be divided into two main parts: objective function and constraints [20]. Thus, its mathematical expression can be described as follows:

(i)SOORPD is defined by the following formula:

$$Min\ \ F(x,u) = f_i(x,u),\ \ i = 1,2,\cdots n \tag{1}$$

(ii)MOORPD is defined by the following formula:

$$Min\ \ F(x,u) = \{f_1(x,u), f_2(x,u),\cdots f_n(x,u)\} \tag{2}$$

(iii)Both SOORPD and MOORPD are subject to the following constraints:

$$\begin{aligned} h_i(x,u) &= 0,\ \ i = 1,2,\cdots hn \\ g_j(x,u) &\le 0,\ \ j = 1,2,\cdots gn \end{aligned} \tag{3}$$

$$\begin{aligned} x &\in [x_{\min}, x_{\max}] \\ u &\in [u_{\min}, u_{\max}] \end{aligned} \tag{4}$$

where $f_1(x,u)$, $f_2(x,u)$ and $f_3(x,u)$ denote the objective function to be optimized; n denotes the number of objective functions; h and g denote the equality constraints and inequality constraints in the reactive power flow equation, respectively; hn and gn denote the maximum number of equality constraints and inequality constraints, respectively. Hence, the vector x of control variables and the vector u of state variables are denoted as follows:

$$x = [V_{G_1} \cdots V_{G_{NPV}}, T_{B_1} \cdots T_{B_{NT}}, Q_{R_1} \cdots Q_{R_{NG}}]^T \tag{5}$$

$$u = [V_{L_1} \cdots V_{L_{NPQ}}, Q_{G_1} \cdots Q_{G_{NPV}}, S_{AB_1} \cdots S_{AB_{NS}}]^T \tag{6}$$

as known from the above equations, the control variables x include: the voltage at the generator bus (V_G), the tap ratio at the transformer (T_B), and reactive power output of reactive power compensation equipment (Q_R); the state variables u include: the voltage at the load bus (V_L), the reactive power output at the generator (Q_G), and the apparent power at the transmission line between buses A and B (S_{AB}); NPV is the number of PV buses, NT is the number of transformers, NG is the number of reactive power compensation devices , NPQ is the number of PQ buses, and NS is the number of network tributaries.

A. Objective Functions

This section discusses the objective functions for the three different optimization objectives used in this study: minimum P_{loss}, minimum V_d, and L_{index}.

1) Minimization of P_{loss}

Considering the economics of power system operation, the P_{loss} as the most classical objective in the ORPD, aims to minimize the to minimize the active power loss in the transmission system, whose mathematical model can be expressed as follows:

$$Minimize\ \ f_1 = \left\{ P_{loss}(x,u) = \sum_{k \in NS} G_k \left(V_i^2 + V_j^2 - 2V_iV_j \cos\left(\delta_i - \delta_j\right)\right)\right\} \tag{7}$$

where G_k is the admittance of branch k; V_i and V_j denote the voltage amplitudes of bus i and bus j, respectively; and δ_i and δ_j denote the phase angles of bus i and bus j, respectively.

2) Minimization of V_d

As an important indicator of power quality, voltage determines the balance and distribution capacity of the power system. Reasonable configuration and optimized operation of reactive equipment can improve voltage quality effectively and ensure system voltage stability. From the perspective of the safety of power system operation and improvement of system voltage distribution, minimization of V_d can also be used as the optimization objective of the ORPD problem, whose formula can be defined as follows:

$$Minimize\ \ f_2 = \left\{ V_d = \sum_{i=1}^{NPQ} \left| V_i - V_{ref} \right| \right\} \tag{8}$$

where V_i denotes the voltage value of the ith PQ bus; and V_{ref} is the ideal voltage with the minimum value of 1 p.u. .

3) Minimization of L_{index}

Voltage stability is closely related to the reactive power of the power system, and continuous changes in the real power consumed by the load can lead to voltage instability, even with irreversible consequences. Therefore, in the optimal reactive power flow, the L_{index} is inevitably affected [21].

When solving the ORPD problem, the L_{index}, as one of the important factors in power system operation planning, should also be considered as an optimization objective for the ORPD problem, in addition to considering the two objectives of P_{loss} and V_d [22, 23]. By reducing the L_{index} of the whole power system, the purpose of improving the system voltage stability is finally achieved [24]. It is necessary to consider the objective function of L_{index} in order to enhance the voltage stability and distance the power system away from the voltage collapse threshold, which is expressed as follows [25]:

$$Minimize \ \ f_3 = \min(L_{index}) \tag{9}$$

$$L_{index} = \max(L_k) = \max(\left|1 - \sum_{i=1}^{NPV} -\left[Y_{VQ}\right]^{-1}\left[Y_{VV}\right]\frac{V_i}{V_k}\right|), \ \ k \in NPQ \tag{10}$$

where V_i denotes the voltage of the ith PV bus; V_k denotes the voltage of the kth PQ bus; Y_{VQ} and Y_{VV} denote the submatrices of the power network conductance matrix after separating the PV and PQ buses as follows:

$$\begin{bmatrix} I_Q \\ I_V \end{bmatrix} = \begin{bmatrix} Y_{QQ} & Y_{QV} \\ Y_{VQ} & Y_{VV} \end{bmatrix} \begin{bmatrix} V_Q \\ V_V \end{bmatrix} \tag{11}$$

as shown in the above formula, the L_{index} value is usually within the range of [0,1]. When the L_{index} value of the load is equal to zero, the power system can operate normally and stably. However, when the L_{index} value is 1, it will lead to an abnormal state of voltage collapse. Therefore, when determining the L_{index} value of the whole system, the stability of the whole power system is measured by the minimum of the maximum value of the L_{index} of the PQ buses.

B. Constraint Condition

The objective functions of the three optimization objectives of the optimal reactive power dispatch problem mentioned in this study are subject to the following power system constraints.

1) Equality Constraints

The following two equality constraints are derived from the power balance equation for power flow calculations:

$$P_{gi} - P_{di} - V_i \sum_{k=1}^{N_W} V_k \left[G_{ik} \cos\delta_{ik} + B_{ik} \sin\delta_{ik}\right] = 0, i \in N_V \tag{12}$$

$$Q_{gi} - Q_{di} - V_i \sum_{k=1}^{N_W} V_k \left[G_{ik} \sin\delta_{ik} - B_{ik} \cos\delta_{ik}\right] = 0, i \in NPQ \tag{13}$$

where P_{gi} and Q_{gi} denote the active power and reactive power input to the ith PV bus respectively; P_{di} and Q_{di} denote the active power and reactive power dissipated by the ith PQ bus respectively; G_{ik} and B_{ik} denote the conductance and the susceptance between the bus i and the bus k in the transmission line, respectively; and N_W denotes the total number of buses connected to the bus i; N_V denotes the number of all buses except the balance bus; N_{PQ} denotes the number of PQ buses.

2) Inequality Constraints

There are inequality constraints below which can be classified into control variable inequality constraints and state variable inequality constraints according to the type of variables, with the following expressions.

a) Control variable inequality constraints

1. Generator terminal voltage limit

$$V_{Gi,\min} \le V_{Gi} \le V_{Gi,\max}, \ \ i = 1, 2, \cdots, NPV \tag{14}$$

2. Transformer tap ratio limitation

$$T_{Bi,\min} \le T_{Bi} \le T_{Bi,\max}, \ \ i = 1, 2, \cdots, NT \tag{15}$$

3. Limit of reactive power output of reactive power compensation equipment

$$Q_{Ri,\min} \le Q_{Ri} \le Q_{Ri,\max}, \ \ i = 1, 2, \cdots, NG \tag{16}$$

b) State variable inequality constraints

1. Reactive power limit of bus PV

$$Q_{Gi,\min} \le Q_{Gi} \le Q_{Gi,\max}, \ \ i = 1, 2, \cdots, NPV \tag{17}$$

2. Voltage limitation of bus PQ

$$V_{Li,\min} \le V_{Li} \le V_{Li,\max}, \ \ i = 1, 2, \cdots, NPQ \tag{18}$$

3. Apparent power limitation

$$S_{ABi} \le S_{ABi,\max}, \ \ i = 1, 2, \cdots, NS \tag{19}$$

The equality constraints are used as a termination condition for the power flow calculation, which mark the end of the power flow calculation when the equality constraints are satisfied; while in the inequality constraints, the control variables can be set within the constraint range, but the state variables require additional processing.

C. Constraint Processing Technology

1) Single-objective Constraint Processing Method

In the past, reconstructing a new mathematical model using penalty functions is the traditional approach to solve the problem of constraint handing of reactive optimization, but it took a lot of time in adjusting the penalty coefficients. Based on the idea of iterative search of the algorithm, this paper adopts a new constraint handling method, "superior strategy". It can effectively solve the problem of variables exceeding upper and lower limits and guide the algorithm to explore the optimal feasible domain. In the iterative process of the algorithm, $x_i(k)$ represents the position of the individual after k iterations, $\varepsilon_i(k)$ represents the best position of the individual as of k iterations, and f is the fitness function. λ is the constraint evaluation function, whose function is to determine whether the individual violates the constraint. The size of $\lambda(x_i(k))$ determines the degree of transgression of the corresponding solution, and the larger the value is, the greater the degree of transgression. The specific process of the strategy is as follows.

(i)When both $\lambda(\varepsilon_i(k))$ and $\lambda(x_i(k+1))$ are equal to zero, compare the values of $f(\varepsilon_i(k))$ and $f(x_i(k+1))$ and select the individual with the smaller value as the kth+1st generation;

(ii)When one of $\lambda(\varepsilon_i(k))$ and $\lambda(x_i(k+1))$ is zero, the individual who does not violate the constraint is selected as the next generation;

(iii)When both $\lambda(\varepsilon_i(k))$ and $\lambda(x_i(k+1))$ are non-zero, compare the values of $\lambda(\varepsilon_i(k))$ and $\lambda(x_i(k+1))$ and select the individual with the smaller value as the next generation, or if they are equal, select randomly.

Based on the above three conditions, not only the optimal individual is found in the search process, but also the problem of constraint violation by variables is addressed. In this case, the objective function is replaced by the fitness function, while the value of individual constraint violation is obtained by the constraint evaluation function. Applying the strategy to the ORPD problem, the relevant mathematical formulation can be expressed as:

$$\lambda(x)=\sum_{i=1}^{NPV}\lambda Q_{gi}(x)+\sum_{j=1}^{NPQ}\lambda V_{dj}(x)+\sum_{k=1}^{NS}\lambda S_k(x) \quad (20)$$

where x denotes the position of the current population individual; $\lambda Q_G(x)$, $\lambda V_L(x)$ and $\lambda S_{AB}(x)$ denote the constraint violation values of the state variables (including the reactive power output of the PV bus, the voltage of the PQ bus and the apparent power of each branch), respectively, taken in the following way:

$$\lambda u=\begin{cases}u_{\min}-u, u<u_{\min}\\ u-u_{\max}, u>u_{\max}\\ 0, otherwise\end{cases} \quad (21)$$

2) Multi-objective Constraint Processing Method

Like the single-objective optimization problem, the iterative process of the initial population in the multi-objective optimization problem also requires the treatment of system constraints. Similarly, the types of constraints handled by the multi-objective optimization problem are also classified into equality and inequality constraints. Unlike the single-objective constraint processing method, this paper adopts the "constraint domination strategy" to deal with the constraints of multi-objective state variables. The process is shown as follows.

Let x_1 and x_2 denote the two sets of control variables, respectively, and the constraint evaluation function be the sum of the transgression limits of each state variable u.

$$\lambda(x)=\sum_{i=1}^{N_D}g_i(x,u) \quad (22)$$

where N_D denotes the number of state variable inequality constraints; g_i denotes the ith inequality constraint.

(i)When $\lambda(x_1)$ is smaller than $\lambda(x_2)$, x_1 dominates x_2 and x_1 is selected as the next generation of population individuals;

(ii)When $\lambda(x_1)$ is greater than $\lambda(x_2)$, x_2 dominates x_1 and x_2 is selected as the next generation of population individuals.

(iii)When $\lambda(x_1)$ and $\lambda(x_2)$ are equal, if both satisfy the following equation:

$$\forall i\in\{1,2,...,m\}: f_i(x_1)\le f_i(x_2) \quad (23)$$

$$\exists j\in\{1,2,...,m\}: f_j(x_1)< f_j(x_2) \quad (24)$$

x_1 dominates x_2, then x_1 is selected as the next generation particle; if not, x_1 and x_2 do not dominate each other, and an individual is randomly selected as the next generation population individual.

The above is the process in which the constraint domination strategy deals with the multi-objective state variable constraints. Through the above three steps, the population individuals will move to the direction closer to the optimal solution and more feasible. This process not only solves the problem of state variables crossing the limit but also can promote the evolution of the population individuals.

III. The Proposed Approach

AO is a novel intelligent algorithm proposed by Laith Abualigah et al. in 2021. It is easy to implement and simple to calculate. It has been used in solving industrial engineering optimization problems [26] and image classification problems [27]. However, AO still has disadvantages such as insufficient local exploration capability and diversity of search space. To address these shortcomings, an IAO is proposed.

A. Overview of the Aquila Optimization Algorithm

AO is inspired by four group behaviors during predation of Aquila birds in North America: 1. expanding the search range by soaring vertically high for birds hunting in flight; 2. attacking prey in low-level air near the ground by contour flight with short gliding attacks; 3. gradually attacking prey by flying low and descending slowly; 4. walking and grabbing prey on land by swooping [28]. The optimization process of this algorithm is divided into four parts: expanded exploration, narrowed exploration, expanded mining and narrowed mining, and the specific formulas are as follows.

1) Expanded Exploration Phase

$$w_1(k+1)=w_{gbest}(k)\times(1-\frac{k}{k_{\max}})+(w_m(k)-w_{gbest}(k)*rand) \quad (25)$$

$$w_m(k)=\frac{1}{N_{Sample}}\sum_{i=1}^{N_{Sample}}w_i(k),\forall j=1,2,\cdots,D_{im} \quad (26)$$

where $w_{gbest}(k)$ denotes the global best solution obtained before the kth iteration; k_{max} is the maximum number of iterations; $w_m(k)$ denotes that at the kth iteration is the average of all current solutions; N_{Sample} and D_{im} denote the number of candidate solutions and the dimensional size of the problem, respectively.

2) Narrowed Exploration Phase

$$w_2(k+1)=w_{gbest}(k)\times Levy(D_{im})+w_r(k)+(H-L)\times rand \quad (27)$$

$$Levy(D_{im})=s\times\frac{\alpha\times\lambda}{|\beta|^{\frac{1}{\mu}}} \quad (28)$$

$$\lambda=(\frac{\Gamma(1+\mu)\times\sin(\frac{\pi\mu}{2})}{\Gamma(\frac{1+\mu}{2})\times\mu\times2^{(\frac{\mu-1}{2})}}) \quad (29)$$

where $Levy(D_{im})$ denotes the Lévy flight distribution function to improve the global search capability; $\Gamma(1+\mu)$ denotes the standard gamma function; s is fixed to a value of 0.01, μ is fixed to a value of 1.5, α and β denote random numbers from 0 to 1; and $w_r(k)$ denotes the random solution among all solutions in the kth iteration.

$$H=R\times\sin(\theta) \quad (30)$$

$$L=R\times\cos(\theta) \quad (31)$$

$$R=R_1+c\times D_1 \quad (32)$$

$$\theta=-d\times D_1+\theta_1 \quad (33)$$

$$\theta_1=\frac{3\times\pi}{2} \quad (34)$$

where c is a small value fixed at 0.00565 and d is a small value fixed at 0.005; R_1 is in the range [1,20]; and D_1 is an integer from 1 to D_{im}.

3) Expanded Mining Phase

$$w_3(k+1)=(w_{gbest}(k)-w_m(k))\times A-rand+((ub-lb)\times rand+lb)\times B \quad (35)$$

where A and B denote the mining adjustment factor, fixed to the lesser of 0.1; ub and lb denote the upper and lower limits, respectively.

4) Narrowed Mining Phase

$$w_4(k+1)=QF\times w_{gbest}(k)-(g_1\times w(k)\times rand)-g_2\times Levy(D_{im})+rand\times g_1 \quad (36)$$

$$QF(k)=k^{\frac{2\times rand-1}{(1-k_{\max})^2}} \quad (37)$$

$$g_1 = 2 \times rand - 1 \tag{38}$$

$$g_2 = 2 \times (1 - \frac{k}{k_{\max}}) \tag{39}$$

where QF represents the value of the function used to balance the search strategy; g_1 represents the various movements of Aquila during prey tracking; and g_2 represents the linearly decreasing value of the flight slope.

B. Proposed IAO

In order to improve the standard AO to jump out of the local optimum and to enhance the global search, this section proposes three strategies to improve AO: probabilistic perturbation strategy, elite group navigation strategy and introduction of the Cauchy operator, and modifications to the algorithm's expanded mining phase and narrowed mining phase.

1) Probabilistic Perturbation Strategy

In the standard AO, the local search and global search processes are controlled with random variables. A reasonable algorithm search process should, in the early stage, perform a stronger global search to quickly locate the range of the global optimum in the search space; in the later stage, it should slightly enhance the local search capability to improve the algorithm's search degree. The introduction of a probabilistic perturbation strategy to balance the weight of local search and global search can achieve better search results. The mathematical expression of the probabilistic perturbation strategy is as follows:

$$p = p_{\max} - p_{\min} \times (k_{\max} - k) / k_{\max} \tag{40}$$

where p_{max} and p_{min} are set to 0.6 and 0.1, respectively; k is the current number of iterations; k_{max} is the maximum number of iterations.

2) Introduction of Cauchy Operator

To address the shortcomings of insufficient diversity in the AO search space and the tendency to fall into the local optimum, the Cauchy variation is employed to increase the diversity of the population, which improves the ability of the algorithm to find the global optimum and increases the search space. In the Cauchy function, there is a maximum value at the origin, which is more widely distributed on both sides. The Cauchy variation can bring a greater perturbation to the current optimum, thus making the range of the Cauchy distribution function wider. Moreover, by using the Cauchy variant at both ends, jumping out of the local optimum is easier. In this paper, we use the effect of the two-end variation of the Cauchy distribution function to optimize the global optimum, so that the algorithm can reach the global optimum faster and better. The standard Cauchy distribution function formula is as follows:

$$f(X) = \frac{1}{\pi}(\frac{1}{X^2 + 1}) \tag{41}$$

Random perturbation using Cauchy variants facilitates the diversity of the population, thus avoiding the algorithm to fall into local optimum and to improve the global optimization capability. The features of the Cauchy distribution give it the ability to generate random numbers away from the origin. It means that the Cauchy variation of Aquila individuals can quickly escape from local extremes. Besides, the low peak of the Cauchy distribution function can shorten the search time of the mutated Aquila individuals around the domain by using this feature. Therefore, after the current optimum is obtained, the variation of the global optimum in this paper is formulated as follows.

$$w_{newgbest} = w_{gbest} \times (1 + Cauchy(0,1)) \tag{42}$$

The formulas for expanded exploration phase and narrowed exploration phase after the introduction of the Cauchy operator are respectively as follows:

$$w_1(k+1) = w_{newgbest}(k) \times (1 - \frac{k}{k_{\max}}) + (w_m(k) - w_{gbest}(k) * rand) \tag{43}$$

$$w_3(k+1) = (w_{newgbest}(k) - w_m(k)) \times \mathrm{A} - rand + ((ub - lb) \times rand + lb) \times \mathrm{B} \tag{44}$$

3) Elite Group Navigation Strategy

To improve the accuracy of the local optimization search again, an elite group navigation strategy was used to update the position of all Aquila individuals. Using the tendency of Aquila that individuals move closer to the best individual in the population to change the position of the Aquila population, it can finally escape from the local optimum quickly. The specific formula is as follows:

$$w_{new} = w \times \left[1 + m \times (w_{pbest} - w)\right] \tag{45}$$

where w denotes all solutions; w_{new} denotes the updated solution; w_{pbest} denotes the individual best solution; m is a random number from 0 to 2, indicating the degree of optimization.

C. Performance Analysis of IAO

1) Single-objective test function simulation experiments

To prove the validity of the improved strategy in the optimization process, four typical benchmark test functions are used in simulation experiments related to the performance of IAO. The four typical benchmark functions include two unimodal test functions and two multimodal test functions. The mathematical definitions, value ranges, global minimum, and algorithm parameter settings of the four test functions are given in TABLE II. Because the distribution and shape of the extreme value of these test functions are different, experiments with these test functions can represent the degree of algorithmic merit. Among them, Sphere and Step are unimodal test functions with only the global minimum value of 0 and no local optimum trap. And the final function value is close to 0 during the search calculation, which indicates the higher the global search accuracy of the algorithm. Ackley and Schwefel are continuous multimodal test functions where there are multiple local minima and the global optimum is 0. The closer the global optimal solution obtained is to 0 during the iterative computation, the better the algorithm is at finding the optimal in the multimodal test function. The four test functions mentioned above can check the performance of the algorithm in different dimensions.

To obtain reliable results, AO and IAO conducted 30 simulations independently on four benchmark test functions and simultaneously recorded the best, worst, mean and standard deviation values obtained from the experiments, which were then analyzed and compared.

As shown in Fig. 1-Fig. 4, comparison graphs of the convergence of AO and IAO in each of the four tested functions are given. It can be found that after improvement by probabilistic perturbation strategy, Cauchy operator and elite group navigation strategy, IAO has better search performance, faster convergence, and great optimization results. As shown in TABLE III, the optimal value, the best,

worst, mean and standard deviation results of IAO obtained are significantly better than the results of AO, and the comprehensive performance of IAO, such as the global search ability and the solution accuracy, is significantly improved. It further proves that the proposed strategy is feasible and efficient for the improvement of AO.

2) Multi-objective test function simulation experiments

To verify again the performance of the improved strategy proposed in this paper in handling the multi-objective problem, four multi-objective test functions are used to test IAO in this section. The information related to the test functions is shown in TABLE IV. In this section of experiments, 20 independent simulation experiments are conducted for different test functions, respectively. The remaining parameters for this experiment are set as follows: at a population size, the maximum number of iterations is set to 300 in ZDT1 and ZDT2 and 500 in ZDT3 and ZDT4; at population size of 100, the maximum number of iterations is set to 500 in ZDT1 and ZDT2 and 600 in ZDT3 and ZDT4.

As shown in Fig. 5-Fig. 12, there are the Pareto plots obtained by IAO for different population size simulation experiments in the above four test functions. The blue color indicates the real Pareto front, and the red color indicates the Pareto front formed by the non-inferior solution obtained by IAO optimization. It can be seen apparently that the non-inferior solution obtained by IAO is uniformly distributed and very close to the true Pareto front. Moreover, the optimized results of IAO are extremely close to the real Pareto frontier regardless of whether the population size is 50 or 100, which greatly demonstrates that IAO has better search ability and potential. In the meanwhile, it further proves the validity and applicability of the improved method proposed in this paper. In summary, IAO shows better optimization performance in solving multi-objective test function problems, so it has great potential in solving complex multi-objective optimization problems.

TABLE I
PSEUDO CODE OF IAO ALGORITHM

Input: Objective function of SOORPD or MOORPD: $F(x,u)=f_i(x,u)$, $i=1,2,\ldots n$; or $F(x,u)=\{f_1(x,u),f_2(x,u),\ldots,f_n(x,u)\}$;
Initial populations generated in the range of control variables;
Set the basic parameters of IAO: k_{max}, N_{Sample}, c, d, etc;
begin: $k=1$
 while $k < k_{max}$
 for ($i=1,2,\ldots, N_{Sample}$) ***do***
 Update the w_m, H, L, $Levy(Dim)$, etc;
 Calculating objective function values and constraint values, recording individual best values w_{pbest} and global best values w_{gbest};
 if k≤(2/3)*k then
 if p<rand then
 Perform expanded exploration phase Eq (43);
 Else
 Perform narrowed exploration phase Eq (46);
 Else
 if p<rand then
 Perform expanded mining phase Eq (44);
 Else
 Perform narrowed mining phase Eq (47);
 end for
 Perform elite group navigation strategy Eq (45);
 $k=k+1$;
 end while
 Application of constraint processing rules to update individual best values w_{pbest} and global best values w_{gbest};
end
Output: The current global best values: w_{gbest}.

TABLE II
DESCRIPTION OF TEST FUNCTION AND PARAMETER SETTING

Function name	Mathematical formulae	Value range	Minimum value	Dimension	Population size	Generations
Sphere	$M_1=\sum_{i=1}^{n}a_i^2$	$a_i=[-100,100]$	0	30	30	50
Step	$M_2=\sum_{i=1}^{n}[a_i+0.5]^2$	$a_i=[-100,100]$	0	30	30	1000
Ackley	$M_3=-20\exp(-0.2\sqrt{n^{-1}\sum_{i=1}^{n}a_i^2})$ $-\exp(n^{-1}\sum_{i=1}^{n}\cos 2\pi a_i)+20+e$	$a_i=[-32,32]$	0	30	100	50
Schwefel	$M_4=\sum_{i=1}^{n}\lvert a_i\rvert+\prod_{i=1}^{n}\lvert a_i\rvert$	$a_i=[-10,10]$	0	30	100	1000

TABLE III
PERFORMANCE EVALUATION RESULTS

Function name	AO				IAO			
	Best	Worst	Mean	Deviation	Best	Worst	Mean	Deviation
Sphere	5.96E-23	8.44E-13	5.18E-14	1.74E-13	1.25E-39	9.98E-23	3.35E-24	1.79E-23
Step	7.65E-07	6.57E-04	6.74E-05	1.54E-04	6.80E-09	9.72E-07	3.37E-07	2.50E-07
Ackley	5.37E-13	9.64E-10	6.84E-11	1.75E-10	8.88E-16	8.88E-16	8.88E-16	0.00E+00
Schwefel	1.55E-161	8.82E-153	3.00E-154	1.58E-153	0.00E+00	0.00E+00	0.00E+00	0.00E+00

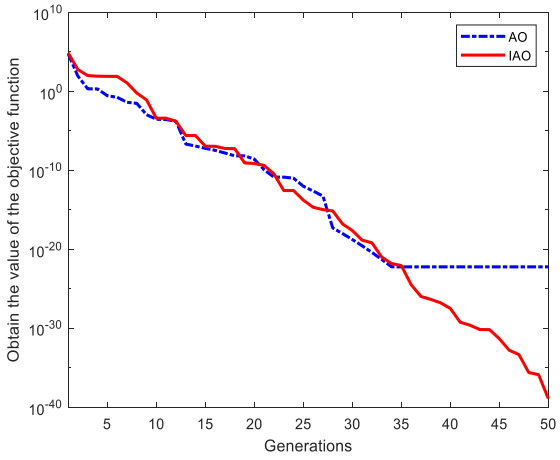

Fig. 1. Convergence curve of Sphere

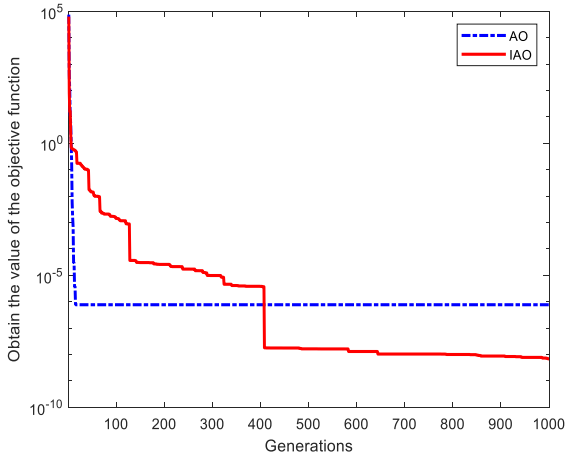

Fig. 2. Convergence curve of Step

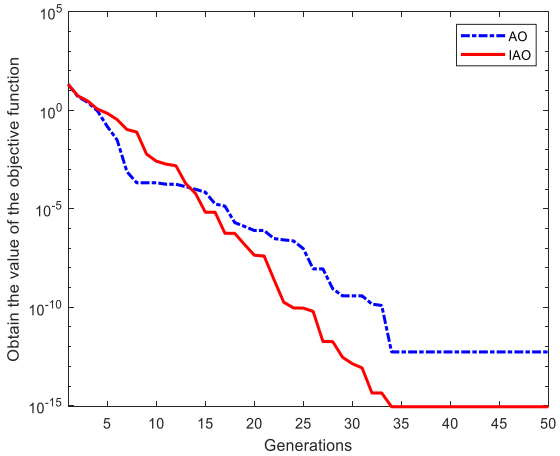

Fig. 3. Convergence curve of Ackley

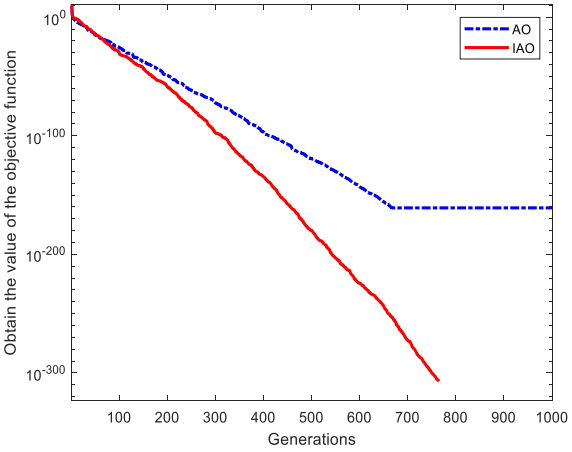

Fig. 4. Convergence curve of Schwefel

TABLE IV
DESCRIPTION OF TEST FUNCTION

Function name	Mathematical formulae	Value range	Dimension
ZDT1	$\begin{cases} M_1(a) = a_1 \\ M_2(a) = N(a)[1-\sqrt{a_1 / N(a)}] \\ N(a) = 1+9(\sum_{i=2}^{n} a_i)/(n-1) \end{cases}$	$a_i \in [0,1]$	30
ZDT2	$\begin{cases} M_1(a) = a_1 \\ M_2(a) = N(a)[1-(a_1 / N(a))^2] \\ N(a) = 1+9(\sum_{i=2}^{n} a_i)/(n-1) \end{cases}$	$a_i \in [0,1]$	30
ZDT3	$\begin{cases} M_1(a) = a_1 \\ M_2(a) = N(a)[1-\sqrt{a_1 / N(a)} - (a_1 / N(a))\sin(10\pi a_1)] \\ N(a) = 1+9(\sum_{i=2}^{n} a_i)/(n-1) \end{cases}$	$a_i \in [0,1]$	30
ZDT4	$\begin{cases} M_1(a) = a_1 \\ M_2(a) = 1-\sqrt{a_1 / N(a)} \\ N(a) = 1+10(n-1)+\sum_{i=2}^{n}(a_i^2 - 10\cos(4\pi a_i)) \end{cases}$	$a_1 \in [0,1]$ $a_i \in [-10,10]$ $i = 2,\ldots,n$	30

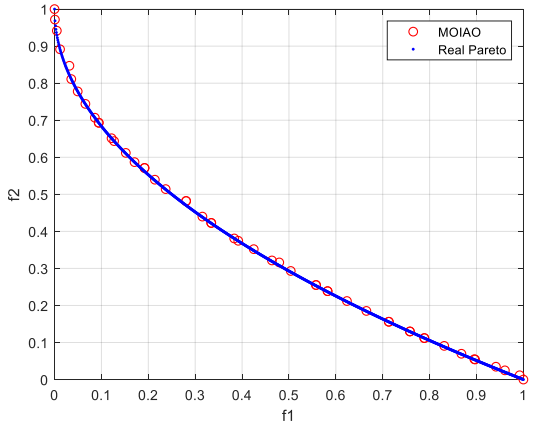

Fig. 5. Pareto curve of ZDT1 at N_{Sample} is 50

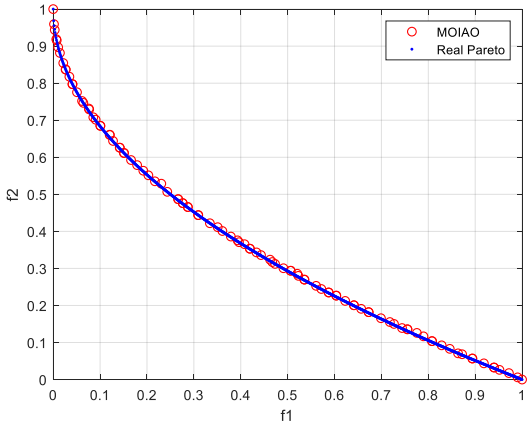

Fig. 6. Pareto curve of ZDT1 at N_{Sample} is 100

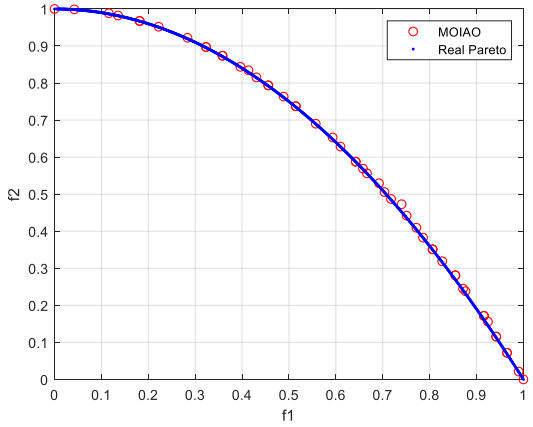

Fig. 7. Pareto curve of ZDT2 at N_{Sample} is 50

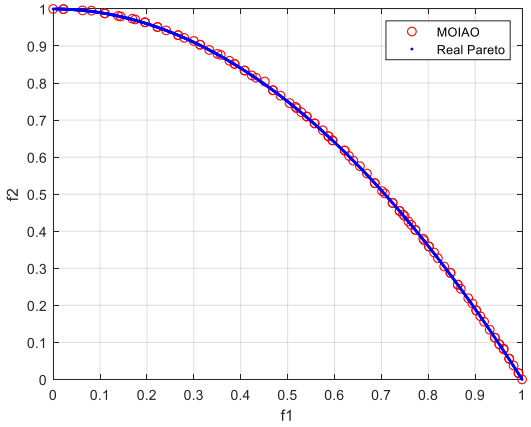

Fig. 8. Pareto curve of ZDT2 at N_{Sample} is 100

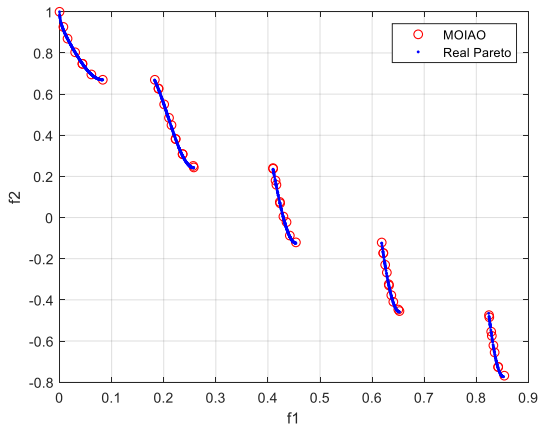

Fig. 9. Pareto curve of ZDT3 at N_{Sample} is 50

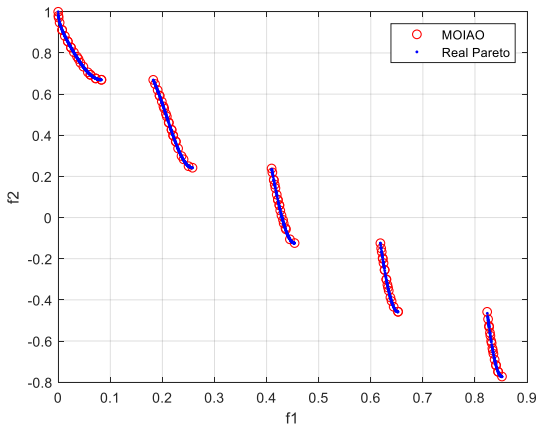

Fig. 10. Pareto curve of ZDT3 at N_{Sample} is 100

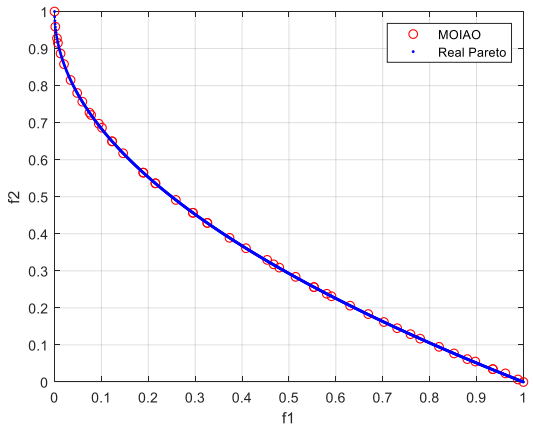

Fig. 11. Pareto curve of ZDT4 at N_{Sample} is 50

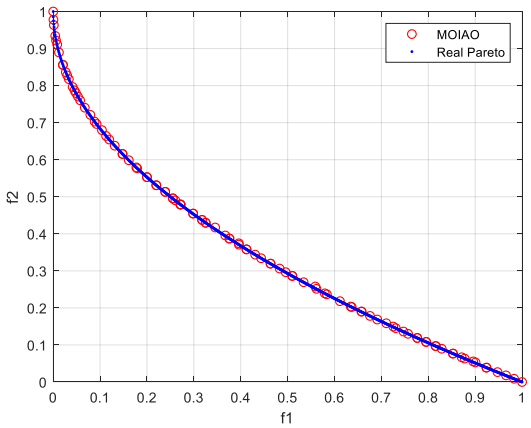

Fig. 12. Pareto curve of ZDT4 at N_{Sample} is 100

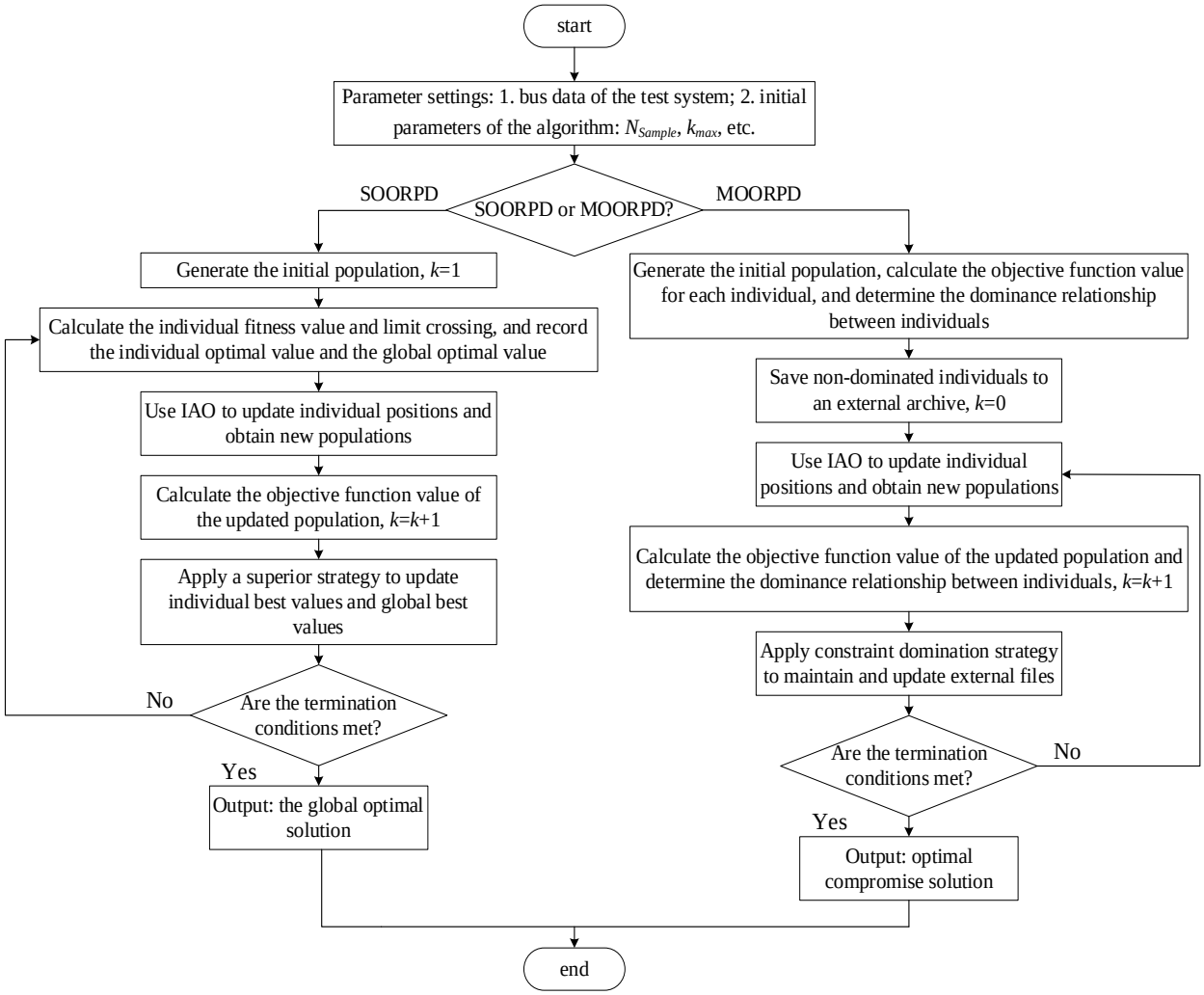

Fig. 13. Process for solving SOORPD and MOORPD problems

TABLE V
SYSTEM DATA OF THE TEST SYSTEM

System Data	IEEE14-bus system	IEEE30-bus system	IEEE57-bus system
Active power of generators (MW)	272.39	289.23	1278.66
Reactive power of generators (MVAr)	82.44	139.10	321.08
Active power demands (MW)	259.00	283.40	1250.80
Reactive power demands (MVAr)	73.50	126.20	336.40
Active power losses (MW)	13.393	5.832	27.864
Reactive power losses (MVAr)	54.54	30.23	121.67

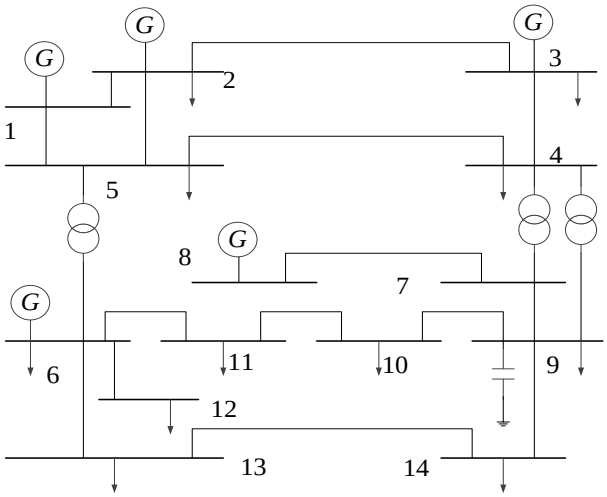

Fig. 14. Structure diagram of IEEE14-bus

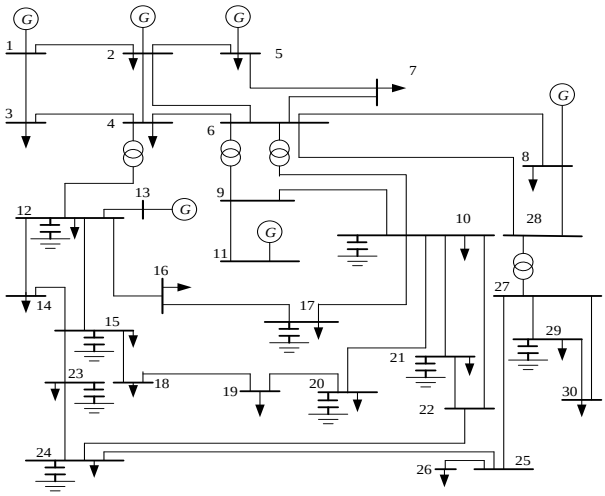

Fig. 15. Structure diagram of IEEE30-bus

TABLE VI
COMPARISON OF SIMULATION RESULTS FOR OPTIMIZED P_{loss} AND V_d

Control variable	GSA	PSO	AO	IAO	Control variable	GSA	PSO	AO	IAO
V_{g1}(p.u.)	1.1000	1.1000	1.1000	1.1000	V_{g1}(p.u.)	1.0521	1.0622	1.0539	1.0599
V_{g2}	1.0773	1.0767	1.0768	1.0767	V_{g2}	1.0308	1.0410	1.0316	1.0404
V_{g3}	1.0519	1.0465	1.0464	1.0463	V_{g3}	0.9999	1.0095	1.0034	1.0114
V_{g6}	1.1000	1.0226	1.0029	1.0634	V_{g6}	1.0216	1.0216	1.0216	1.0172
V_{g8}	1.1000	1.0878	1.0696	1.0930	V_{g8}	1.0420	1.0312	1.0446	1.0349
$T_{4\text{-}7}$	0.9400	0.9800	1.0000	1.0400	$T_{4\text{-}7}$	1.0000	0.9200	1.0000	1.0400
$T_{4\text{-}9}$	0.9000	1.1000	0.9800	0.9000	$T_{4\text{-}9}$	0.9400	1.0400	0.9600	0.9000
$T_{5\text{-}6}$	0.9600	1.0400	1.0800	1.0000	$T_{5\text{-}6}$	0.9400	0.9400	0.9600	0.9200
Q_{c9}(p.u.)	0.0450	0.0500	0.0450	0.0500	Q_{c9}(p.u.)	0.0350	0.0500	0.0450	0.0500
P_{loss}(MW)	12.5043	12.4466	12.5516	**12.3978**	V_d(p.u.)	0.0514	0.0677	0.0498	**0.0337**

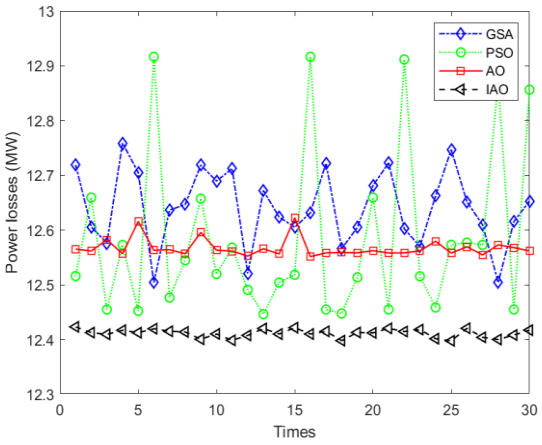

Fig. 16. Distribution of experimental results of optimized P_{loss}

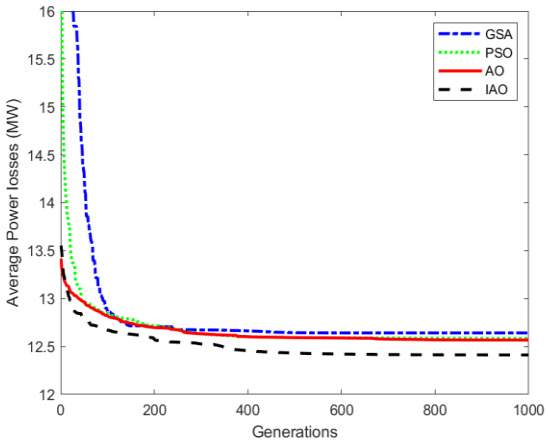

Fig. 19. Average convergence curve of optimized P_{loss}

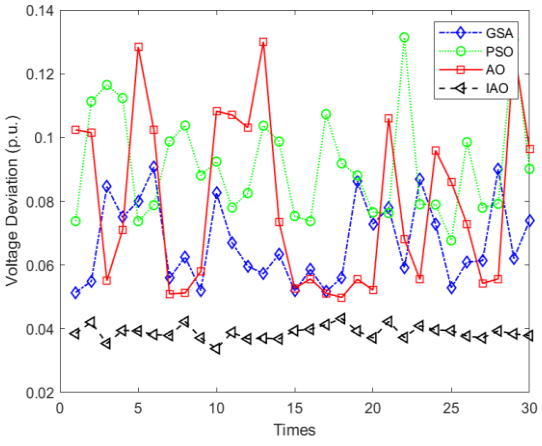

Fig. 17. Distribution of experimental results of optimized V_d

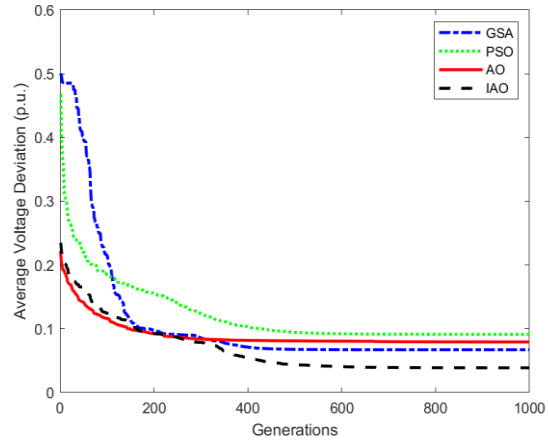

Fig. 20. Average convergence curve of optimized V_d

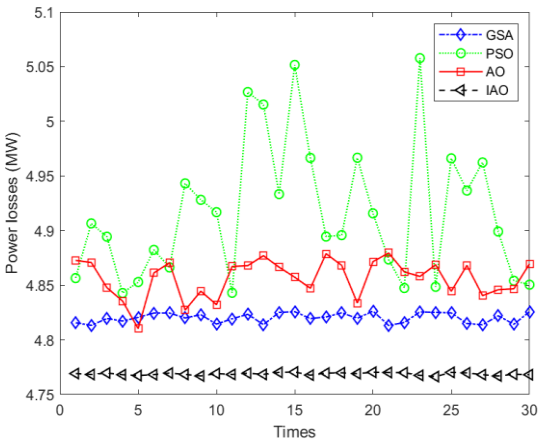

Fig. 18. Distribution of experimental results of optimized P_{loss}

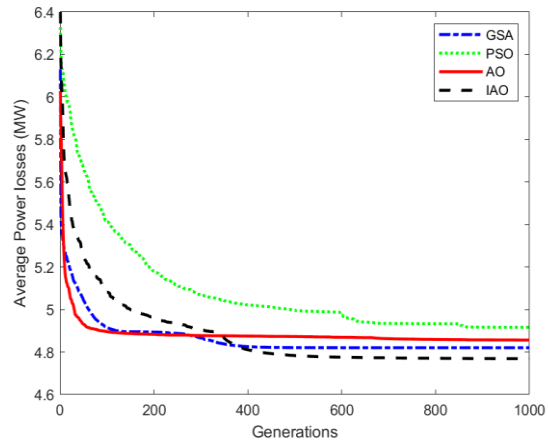

Fig. 21. Average convergence curve of optimized P_{loss}

TABLE VII
COMPARISON OF SIMULATION RESULTS FOR OPTIMIZED P_{loss} AND V_d

Control variable	GSA	PSO	AO	IAO	Control variable	GSA	PSO	AO	IAO
V_{g1}(p.u.)	1.0806	1.0824	1.082159	1.0821	V_{g1}(p.u.)	1.0127	1.0176	1.0096	1.0055
V_{g2}	1.0717	1.0730	1.0728	1.0729	V_{g2}	1.0095	1.0174	1.0069	1.0016
V_{g5}	1.0497	1.0505	1.0502	1.0511	V_{g5}	1.0206	1.0151	1.0201	1.0185
V_{g8}	1.0504	1.0507	1.0511	1.0510	V_{g8}	1.0082	1.0074	1.0075	1.0081
V_{g11}	1.1000	1.1000	1.0938	1.0971	V_{g11}	1.0408	1.0879	1.0401	1.0403
V_{g13}	1.0719	1.0465	1.0655	1.0597	V_{g13}	1.0152	0.9910	1.0308	1.0214
$T_{6\text{-}9}$	1.0120	0.9760	1.0000	1.0720	$T_{6\text{-}9}$	0.9920	1.1000	1.0260	1.0580
$T_{6\text{-}10}$	0.9840	1.1000	1.0040	0.9120	$T_{6\text{-}10}$	0.9360	0.9000	0.9020	0.9000
$T_{4\text{-}12}$	0.9980	1.0100	0.9920	0.9840	$T_{4\text{-}12}$	0.9740	0.9380	0.9940	1.0020
$T_{28\text{-}27}$	0.9880	0.9860	0.9880	0.9760	$T_{28\text{-}27}$	0.9640	0.9660	0.9580	0.9700
Q_{c10}(p.u.)	0.0205	0.0000	0.0360	0.0210	Q_{c10}(p.u.)	0.0215	0.0000	0.0110	0.0495
Q_{c12}	0.0325	0.0500	0.0450	0.0320	Q_{c12}	0.0280	0.0000	0.0160	0.0235
Q_{c15}	0.0310	0.0500	0.0285	0.0440	Q_{c15}	0.0310	0.0500	0.0255	0.0500
Q_{c17}	0.0260	0.0000	0.0410	0.0485	Q_{c17}	0.0265	0.0500	0.0190	0.0015
Q_{c20}	0.0245	0.0470	0.0205	0.0360	Q_{c20}	0.0305	0.0000	0.0475	0.0500
Q_{c21}	0.0250	0.0500	0.0245	0.0495	Q_{c21}	0.0230	0.0500	0.0345	0.0475
Q_{c23}	0.0330	0.0315	0.0295	0.0260	Q_{c23}	0.0315	0.0500	0.0175	0.0500
Q_{c24}	0.0290	0.0500	0.0330	0.0500	Q_{c24}	0.0345	0.0500	0.0270	0.0495
Q_{c29}	0.0300	0.0000	0.0260	0.0235	Q_{c29}	0.0350	0.0220	0.0325	0.0315
P_{loss}(MW)	4.8132	4.8429	4.8103	**4.7664**	V_d(p.u.)	0.1321	0.1191	0.1240	**0.0887**

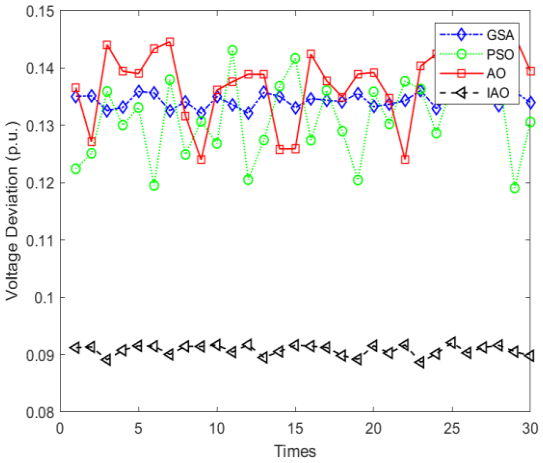

Fig. 22. Distribution of experimental results of optimized L_{index}

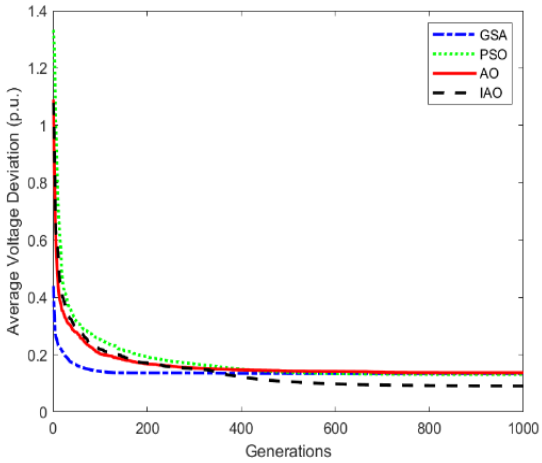

Fig. 23. Average convergence curve of optimized L_{index}

TABLE VIII
OPTIMIZATION OF THE BEST COMPROMISE SOLUTION AND CONTROL VARIABLES OBTAINED

Control variable	MOPSO	MOAO	MOIAO	MOIPSO[29]	Control variable	MOPSO	MOAO	MOIAO	GBICA[30]
V_{g1}(p.u.)	1.1000	0.9816	1.0453	0.9057	V_{g1}(p.u.)	1.1000	1.1000	1.0526	1.6036
V_{g2}	1.1000	0.9773	1.1000	0.9616	V_{g2}	0.9500	1.1000	1.0305	1.0566
V_{g5}	1.1000	0.9768	1.0613	0.9068	V_{g5}	0.9500	1.1000	0.9817	1.0273
V_{g8}	0.9500	0.9777	1.1000	0.9511	V_{g8}	1.1000	1.1000	1.0959	1.0258
V_{g11}	1.1000	0.9720	0.9941	1.0659	V_{g11}	0.9500	1.1000	0.9550	1.0279
V_{g13}	1.1000	0.9784	0.9978	1.1000	V_{g13}	1.1000	1.1000	1.0732	1.0104
$T_{6\text{-}9}$	0.9763	0.9550	0.9740	0.9300	$T_{6\text{-}9}$	1.0836	1.0030	1.0765	1.0100
$T_{6\text{-}10}$	0.9000	0.9505	0.9001	1.1000	$T_{6\text{-}10}$	0.9000	1.0060	0.9004	1.0300
$T_{4\text{-}12}$	0.9418	0.9715	0.9378	1.1000	$T_{4\text{-}12}$	1.0215	1.0463	1.0232	0.9700
$T_{28\text{-}27}$	0.9230	0.9272	0.9103	0.9500	$T_{28\text{-}27}$	0.9793	0.9711	0.9773	0.9800
Q_{c10}(p.u.)	0.0500	0.0372	0.0500	0.1300	Q_{c10}(p.u.)	0.0000	0.0500	0.0000	0.1700
Q_{c12}	0.0500	0.0158	0.0499	0.0300	Q_{c12}	0.0000	0.0325	0.0000	-
Q_{c15}	0.0500	0.0465	0.0499	0.0800	Q_{c15}	0.0140	0.0500	0.0259	-
Q_{c17}	0.0500	0.0500	0.0500	0.0000	Q_{c17}	0.0500	0.0500	0.0493	-
Q_{c20}	0.0500	0.0464	0.0499	0.0300	Q_{c20}	0.0413	0.0500	0.0409	-
Q_{c21}	0.0500	0.0500	0.0500	0.1200	Q_{c21}	0.0500	0.0500	0.0500	-
Q_{c23}	0.0500	0.0237	0.0471	0.0400	Q_{c23}	0.0500	0.0209	0.0288	-
Q_{c24}	0.0500	0.0500	0.0500	0.0000	Q_{c24}	0.0500	0.0500	0.0500	0.1300
Q_{c29}	0.0500	0.0373	0.0294	0.0200	Q_{c29}	0.0234	0.0170	0.0220	-
P_{loss}(MW)	5.1381	5.1411	**5.1373**	5.2150	P_{loss}(MW)	5.1411	5.1479	**5.1388**	5.2063
L_{index}	0.1327	0.1357	**0.1319**	0.1264	V_d(p.u.)	0.2417	0.2761	**0.2385**	0.2627

Remark: - indicates that the corresponding literature does not provide specific values.

TABLE IX
COMPARISON OF SIMULATION RESULTS FOR OPTIMIZED P_{loss} AND V_d

Control variable	GSA	PSO	AO	IAO	Control variable	GSA	PSO	AO	IAO
V_{g1}(p.u.)	1.1000	1.1000	1.1000	1.1000	V_{g1}(p.u.)	1.0125	1.0273	1.0200	1.011
V_{g2}	1.0972	1.1000	1.0995	1.0992	V_{g2}	0.9953	1.0089	1.0241	0.9942
V_{g3}	1.0834	1.0886	1.0899	1.0893	V_{g3}	0.9994	1.0065	1.0104	1.0054
V_{g6}	1.0728	1.0818	1.0829	1.0828	V_{g6}	1.0070	1.0106	1.0031	1.0117
V_{g8}	1.0919	1.1000	1.1000	1.1000	V_{g8}	1.0465	1.0528	1.0338	1.0454
V_{g9}	1.0791	1.0841	1.0866	1.0841	V_{g9}	1.0235	1.0251	1.0200	1.0250
V_{g12}	1.0759	1.0773	1.0833	1.0795	V_{g12}	1.0158	1.0042	1.0255	1.0195
$T_{4\text{-}18}$	0.9700	1.0500	0.9900	1.1000	$T_{4\text{-}18}$	1.0000	1.0273	0.9700	0.9700
$T_{4\text{-}18}$	1.0100	0.9000	1.0000	0.9500	$T_{4\text{-}18}$	1.0000	1.0089	0.9800	0.9800
$T_{21\text{-}20}$	0.9800	1.0000	0.9800	1.0700	$T_{21\text{-}20}$	0.9800	1.1000	0.9700	0.9800
$T_{24\text{-}25}$	0.9900	0.9000	1.0100	1.0300	$T_{24\text{-}25}$	0.9700	0.9000	0.9200	0.9400
$T_{24\text{-}25}$	0.9400	1.1000	0.9800	0.9500	$T_{24\text{-}25}$	0.9500	0.9700	0.9700	1.1000
$T_{24\text{-}26}$	1.0200	1.1000	1.0100	1.0200	$T_{24\text{-}26}$	1.0400	0.9800	0.9800	1.0000
$T_{7\text{-}29}$	0.9700	1.0700	1.0000	0.9900	$T_{7\text{-}29}$	0.9900	1.0100	0.9800	1.0100
$T_{34\text{-}32}$	0.9900	0.9500	1.0000	0.9400	$T_{34\text{-}32}$	0.9300	1.0100	0.9400	0.9300
$T_{11\text{-}41}$	0.9900	0.9000	0.9800	0.9200	$T_{11\text{-}41}$	0.9000	0.9800	0.9000	0.9000
$T_{15\text{-}45}$	0.9800	0.9800	0.9900	0.9800	$T_{15\text{-}45}$	0.9200	0.9200	0.9600	0.9600
$T_{14\text{-}46}$	0.9700	0.9600	1.0100	0.9600	$T_{14\text{-}46}$	0.9400	0.9000	0.9400	0.9200
$T_{10\text{-}51}$	0.9900	0.9700	1.0100	0.9700	$T_{10\text{-}51}$	0.9700	0.9000	0.9800	1.0100
$T_{13\text{-}49}$	0.9600	0.9000	1.0200	0.9300	$T_{13\text{-}49}$	0.9500	0.9900	0.9200	0.9100
$T_{11\text{-}43}$	0.9900	1.1000	1.0400	0.9700	$T_{11\text{-}43}$	0.9800	0.9900	0.9900	1.0100
$T_{40\text{-}56}$	0.9900	0.9000	1.0200	1.000	$T_{40\text{-}56}$	1.0100	0.9000	0.9700	0.9500
$T_{39\text{-}57}$	0.9700	1.1000	1.0100	0.9700	$T_{39\text{-}57}$	0.9400	1.0000	0.9800	0.9200
$T_{9\text{-}55}$	0.9900	1.1000	1.0000	0.9900	$T_{9\text{-}55}$	0.0500	0.9000	0.9800	1.0000
Q_{c18}(p.u.)	0.0850	0.0000	0.0900	0.0100	Q_{c18}(p.u.)	0.1100	0.9700	0.0400	0.0350
Q_{c25}	0.1020	0.1080	0.1260	0.0960	Q_{c25}	0.0550	0.9900	0.0650	0.1400
Q_{c53}	0.0960	0.1800	0.0780	0.1140	Q_{c53}	0.1260	0.0000	0.0180	0.1740
P_{loss}(MW)	22.5085	23.0471	22.8777	**22.2123**	V_d(p.u.)	0.7047	0.7022	0.7922	**0.6513**

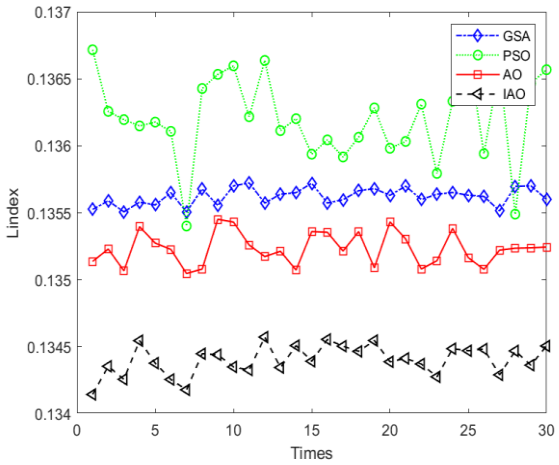

Fig. 24. Distribution of experimental results of optimized L_{index}

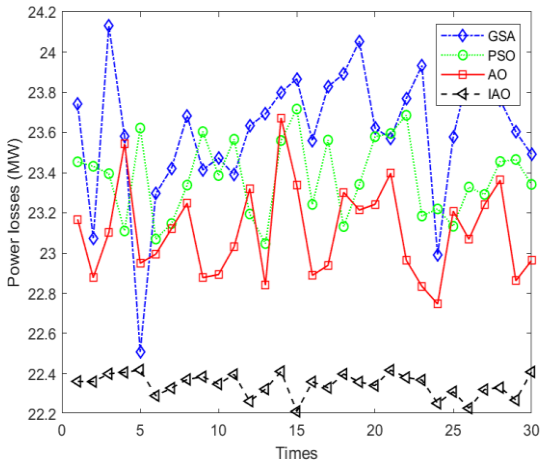

Fig. 26. Distribution of experimental results of optimized P_{loss}

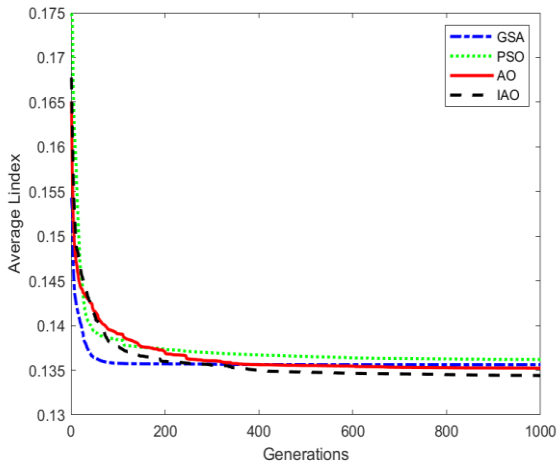

Fig. 25. Average convergence curve of optimized L_{index}

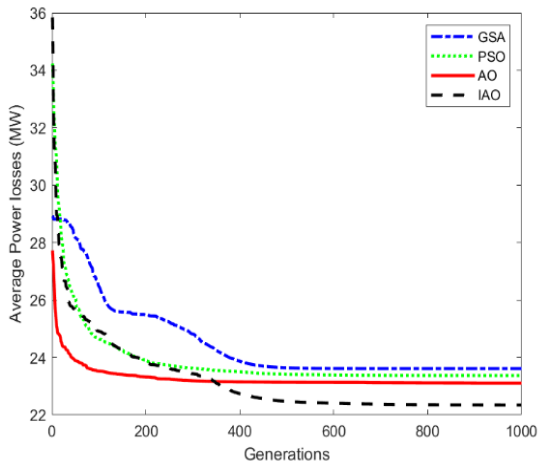

Fig. 27. Average convergence curve of optimized P_{loss}

TABLE X
COMPARISON OF SIMULATION RESULTS FOR OPTIMIZED P_{loss}

Control variable	GSA	AO	IAO	Control variable	GSA	AO	IAO
V_{g1}(p.u.)	0.9951	1.0262	1.0401	V_{g89}	1.0391	1.0600	1.0600
V_{g4}	1.0188	1.0522	1.0544	V_{g90}	1.0037	1.0397	1.0456
V_{g6}	1.0087	1.0414	1.0448	V_{g91}	1.0027	1.0386	1.0471
V_{g8}	1.0335	1.0468	1.0441	V_{g92}	1.0199	1.0551	1.0581
V_{g10}	1.0251	1.0504	1.0531	V_{g99}	0.9941	1.0378	1.0555
V_{g12}	1.0063	1.0373	1.0463	V_{g100}	1.0115	1.0546	1.0600
V_{g15}	1.0020	1.0315	1.0464	V_{g103}	1.0022	1.0485	1.0529
V_{g18}	1.0122	1.0288	1.0502	V_{g104}	1.0012	1.0384	1.0446
V_{g19}	1.0041	1.0287	1.0464	V_{g105}	0.9988	1.0373	1.0449
V_{g24}	1.0133	1.0495	1.0502	V_{g107}	0.9910	1.0217	1.0381
V_{g25}	1.0143	1.0600	1.0600	V_{g110}	0.9899	1.0436	1.0463
V_{g26}	1.0067	1.0561	1.0599	V_{g111}	1.0035	1.0528	1.0503
V_{g27}	1.0045	1.0346	1.0339	V_{g112}	0.9757	1.0302	1.0337
V_{g31}	0.9983	1.0264	1.0349	V_{g113}	1.0147	1.0437	1.0564
V_{g32}	1.0032	1.0333	1.0367	V_{g116}	1.0181	1.0486	1.0484
V_{g34}	0.9965	1.0382	1.0559	$T_{8\text{-}5}$	1.0100	1.0200	0.9800
V_{g36}	0.9848	1.0389	1.0521	$T_{26\text{-}25}$	1.0200	1.0200	1.0000
V_{g40}	0.9947	1.0244	1.0374	$T_{30\text{-}17}$	1.0000	1.0100	0.9800
V_{g42}	0.9959	1.0335	1.0420	$T_{38\text{-}37}$	0.9800	1.0100	0.9700
V_{g46}	1.0043	1.0403	1.0420	$T_{63\text{-}59}$	1.0000	1.0100	0.9900
V_{g49}	1.0110	1.0587	1.0583	$T_{64\text{-}61}$	1.0000	1.0100	0.9700
V_{g54}	0.9946	1.0377	1.0377	$T_{65\text{-}66}$	1.0000	1.0000	0.9900
V_{g55}	0.9941	1.0369	1.0364	$T_{68\text{-}69}$	0.9900	1.0100	1.0000
V_{g56}	0.9932	1.0366	1.0365	$T_{81\text{-}80}$	0.9900	1.0000	0.9900
V_{g59}	1.0066	1.0519	1.0579	C_5(p.u.)	-0.1500	-0.1600	-0.1100
V_{g61}	0.9857	1.0483	1.0595	C_{34}	0.1800	0.1700	0.1400
V_{g62}	0.9722	1.0450	1.0560	C_{37}	-0.1700	-0.1800	-0.1400
V_{g65}	1.0298	1.0519	1.0515	C_{44}	0.1700	0.1700	0.1300
V_{g66}	1.0170	1.0600	1.0600	C_{45}	0.1300	0.1600	0.1100
V_{g69}	1.0388	1.0599	1.0600	C_{46}	0.1200	0.1700	0.1300
V_{g70}	1.0048	1.0393	1.0393	C_{48}	0.1700	0.1700	0.1400
V_{g72}	1.0101	1.0402	1.0408	C_{74}	0.1200	0.1700	0.1100
V_{g73}	0.9998	1.0425	1.0412	C_{79}	0.1600	0.1700	0.1200
V_{g74}	0.9968	1.0299	1.0268	C_{82}	0.1400	0.1700	0.1200
V_{g76}	0.9898	1.0336	1.0242	C_{83}	0.1500	0.1700	0.1300
V_{g77}	1.0083	1.0398	1.0455	C_{105}	0.1500	0.1700	0.1300
V_{g80}	1.0170	1.0491	1.0570	C_{107}	0.1400	0.1600	0.1200
V_{g85}	1.0075	1.0528	1.0571	C_{110}	0.1600	0.1700	0.1200
V_{g87}	1.0194	1.0452	1.0436	P_{loss}(MW)	125.6977	116.0602	**115.0060**

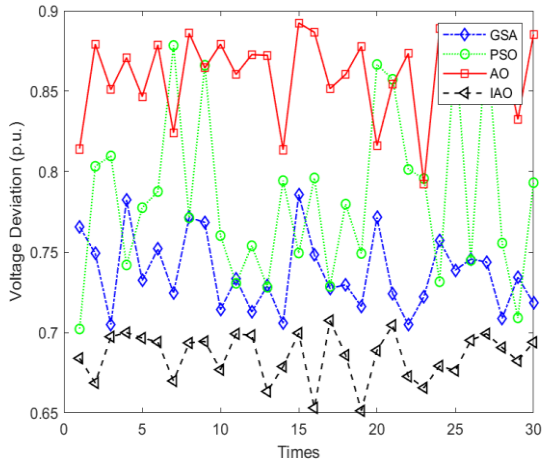

Fig. 28. Distribution of experimental results of optimized V_d

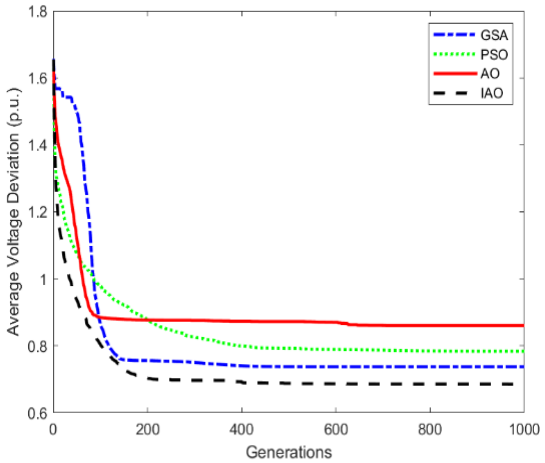

Fig. 29. Average convergence curve of optimized V_d

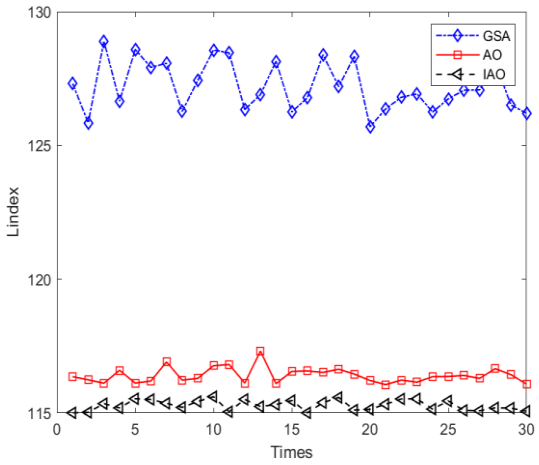

Fig. 30. Distribution of experimental results of optimized P_{loss}

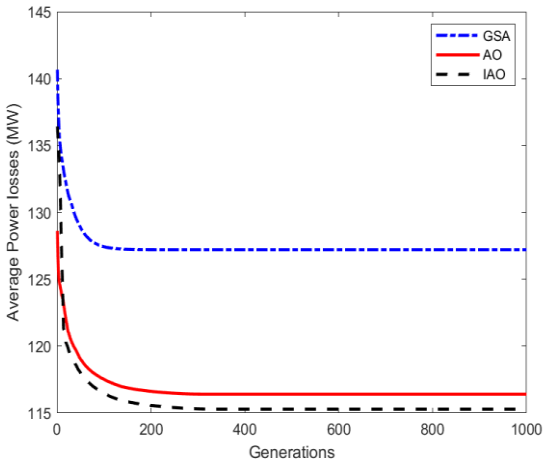

Fig. 31. Average convergence curve of optimized P_{loss}

Finally, in the standard Aquila optimization algorithm, the two stages of the expanded mining phase and narrowed mining phase still have certain defects and are prone to fall into local optimum. Based on not changing the principles of the standard algorithm, these two stages are modified by the following equations:

$$w_2(k+1) = w_{gbest}(k) + (Levy(D_{im}) \times w_r(k)) \times (H - L) \times rand \quad (46)$$

$$w_4(k+1) = w_{gbest}(k) + [QF \times (g_1 \times w(k) \times rand) \times g_2 \times Levy(D_{im})] \times rand \times g_1 \quad (47)$$

The IAO pseudo-code is shown in TABLE I.

IV. Simulation Results and Analysis

In this section, to demonstrate the validity of the improved strategy, SOORPD simulation experiments are performed on four standard test systems of different sizes and MOORPD simulation experiments are performed on the IEEE30-bus test system. Thus, the capability of the proposed improved algorithm can be tested by synthesizing comprehensive numerical values, then make a comparison between the obtained results and other realized algorithms. The process of the proposed method to deal with the ORPD problem is shown in Fig. 13. It should be seen that the proposed method has been coded on matlab2019a and a PC with a 3.40 GHz processor and 16 GB RAM. The data of the three standard test systems are presented in this section, and the specific relevant data are detailed in the literature [31] and literature [18].

A. Parameter Setting

The systems selected for this section are the power test systems commonly used to study the optimal flow problems in power systems. The system data of some test systems are detailed in TABLE V.

For the complexity of the power system network structure and the high dimensionality of the power flow problem itself, it is crucial to set the appropriate number of iterations and initial population size. For example, a larger population size provides better assurance of particle diversity, but it can also lead to increased computing complexity of the algorithm. Conversely, the computational complexity will be reduced but not guarantee the diversity of the population, while the increase in population diversity means that the algorithm has a greater possibility of searching for a better solution. To ensure that the set parameters fully achieve convergence, repeated experiments and results are analyzed. Therefore, in the SOORPD problem, the number of iterations is set to 1000 and the initial population size is set to 30, and in the MOORPD problem, the number of iterations is set to 300. In addition, the initial population size is set to 100.

B. IEEE14-bus Test System

Fig. 14 shows the internal structure of the IEEE 14-bus system. TABLE XI gives the important parameter limitations of the system.

TABLE XI
Limits of Reactive Power of Generators in IEEE14-Bus Test System

Bus number	$Q_{gi,min}$ (MVAr)	$Q_{gi,max}$ (MVAr)
1	0	10
2	-40	50
3	0	40
6	-6	24
8	-6	24

TABLE XII
Comparison with Literature Results

Method	P_{loss}(MW)	V_d(p.u.)
IAO	**12.3978**	**0.0337**
GSA-CSS[18]	12.5099	0.0383
IGSA-CSS[18]	-	0.0383
GSAPSO[31]	12.4490	-
MTLA-DDE[32]	12.8978	0.0339
DE[33]	13.2390	-

1) P_{loss}

In the first case, only the objective function of the active power transmission losses (P_{loss}) is considered. TABLE VI shows the best results of ORPD obtained by IAO, standard AO, and classical algorithms. Fig. 16 gives the distribution of the results of 30 independent experiments for the four optimization algorithms, and it can be known the distribution of the results of IAO has a smaller distribution range. It is more stable and has a better performance compared to the other algorithms. The average convergence curves of the four optimization algorithms are given in Fig. 19. It is important to note that 30 independent experiments were conducted for each optimization algorithm. It can be noticed that the proposed IAO obtains the smallest P_{loss} optimization value

(12.3978 MW), which is reduced by 0.1065 MW, 0.0488 MW and 0.1538 MW compared to GSA, PSO and AO, respectively. Although these values are small, they cannot be ignored in the overall grid dispatch operation. TABLE XII displays the results obtained in recent years by different methods proposed by scholars, and it is clear that the method proposed in this paper is reliable.

2) V_d

In this subsection, only the objective function of the voltage deviation (V_d) is considered. Again, for each optimization algorithm, the number of independent experiments is set to 30. The comparison of the results with the other algorithms is shown in Fig. 20 and TABLE VI. It can be noticed that the optimal value of V_d obtained by IAO (0.0337 p.u.) is much smaller than the optimal value of the other algorithms, indicating the superiority of the algorithm. As is seen in TABLE XII, the algorithm obtains an advantage in optimizing the V_d. The distribution of the experimental results shown in Fig. 17 demonstrates the stability of IAO more effectively.

C. IEEE30-bus Test System

Fig. 15 shows the internal structure of the IEEE 30-bus system. TABLE XIII gives the important parameter limitations of the system.

TABLE XIII
LIMITS OF REACTIVE POWER OF GENERATORS IN IEEE30-BUS TEST SYSTEM

Bus number	$Q_{gi,min}$ (MVAr)	$Q_{gi,max}$ (MVAr)
1	-20	200
2	-20	100
5	-15	80
8	-15	60
11	-10	50
13	-15	60

TABLE XIV
COMPARISON WITH LITERATURE RESULTS

Method	P_{loss}(MW)	V_d(p.u.)
IAO	**4.7664**	**0.0887**
HAS[17]	4.9059	0.1349
SGA[17]	4.9408	0.1501
GSA-CSS[18]	4.7930	0.1239
IGSA-CSS[18]	-	0.0897
TS[34]	4.9203	0.1540
FA[35]	4.7694	1.9542

1) P_{loss}

In the first case, IAO is applied to deal with the P_{loss} optimization problem of the IEEE30-bus test system. Fig. 21 is the average convergence curves of the four optimization algorithms, IAO, GSA, PSO and AO under 1000 iterations. It demonstrates that the average convergence curve of IAO has a lower average convergence curve than the other three algorithms. The optimal value of P_{loss} obtained by each algorithm and the optimization scheme corresponding to the control variables are given in TABLE VII, where IAO reduces the P_{loss} of the test system from 5.832 MW to 4.7664 MW with a loss reduction rate of 18.27%. Compared with the loss reduction rate of the comparison algorithms, IAO improves the loss reduction rate by 0.8%, 1.31%, and 0.75% over GSA, PSO, and AO, respectively. The distribution of optimization results of the four algorithms for 30 experiments provided in Fig. 18 easily shows that IAO has a lower distribution position and less fluctuation. It demonstrates that IAO is more advantageous in optimizing the P_{loss}. TABLE XIV presents the results received from the different methods proposed during recent years, which proves that the method proposed in this paper is plausible.

2) V_d

In this case, Fig. 22 gives the optimization results of the minimum V_d of the four algorithms for 30 experiments. According to the distribution, it is seen that IAO obtains a much lower distribution position of the minimum V_d than the other three algorithms and has better stability. The average convergence curves of the four algorithms for 30 experiments are given in Fig. 23, it can be visualized that IAO has a better convergence. TABLE VII gives the control variable scheme for the optimal results. The optimal V_d value obtained by IAO is 0.0887, which is 0.0434, 0.0304, and 0.0353 lower than the optimal results of the other three algorithms, respectively. It shows that IAO is more competitive in optimizing the V_d compared to the other three algorithms. Further, as shown in TABLE XIV, the algorithm is more advantageous in optimizing the V_d.

TABLE XV
COMPARISON OF SIMULATION RESULTS FOR OPTIMIZED L_{index}

Control variable	GSA	PSO	AO	IAO
V_{g1}(p.u.)	1.0671	1.1000	1.0731	1.0701
V_{g2}	1.0577	1.0633	1.0692	1.0618
V_{g5}	1.0509	1.0186	1.0771	1.0696
V_{g8}	1.0295	1.0236	1.0487	1.0575
V_{g11}	1.0784	1.0736	1.1000	1.0981
V_{g13}	1.0662	1.1000	1.0773	1.0833
$T_{6\text{-}9}$	0.9700	0.9680	1.0420	1.0280
$T_{6\text{-}10}$	0.9940	0.9000	1.0560	0.9120
$T_{4\text{-}12}$	0.9640	1.1000	0.9960	1.0140
$T_{28\text{-}27}$	0.9480	0.9520	0.9680	0.9620
Q_{c10}(p.u.)	0.0270	0.0000	0.0415	0.0070
Q_{c12}	0.0320	0.0500	0.0360	0.0030
Q_{c15}	0.0345	0.0500	0.0270	0.0420
Q_{c17}	0.0290	0.0000	0.0405	0.0240
Q_{c20}	0.0245	0.0500	0.0175	0.0330
Q_{c21}	0.0200	0.0000	0.0440	0.0110
Q_{c23}	0.0310	0.0135	0.0445	0.0210
Q_{c24}	0.0275	0.0000	0.0390	0.0085
Q_{c29}	0.0280	0.0500	0.0270	0.0055
L_{index}	0.1355	0.1354	0.1350	**0.1341**

3) L_{index}

In the third case, to verify the validity of the proposed IAO again, the optimization experiment of the L_{index} in the test system is continued. The classical GSA, PSO, and AO are still used for comparison experiments, and the independent experiments of each algorithm are still set to 30 times. The comparison of the optimization results is shown in Fig. 24 and Fig. 25. The original AO has an advantage over GSA and PSO in optimizing the L_{index}, while the improved IAO further improves the voltage stability on the basis of AO. As it is shown in TABLE XV that the best L_{index} value achieved by IAO is 0.1341, which is lower compared to the other three algorithms and easier to stay away from the voltage collapse point.

4) Multi-objective Reactive Power Optimization Dispatch

The SOORPD problem focuses on finding a global optimum with a single objective function. However, the

MOORPD problem requires simultaneous optimization of several conflicting and mutually constraining objective functions. The objectives of SOORPD are minimum P_{loss}, minimum V_d, and L_{index}. In previous experiments, each objective was optimized separately. To further confirm the validity of the proposed IAO, the multi-objective IAO (MOIAO) is applied to the problem of ORPD. Therefore, three different cases are considered in this section as follows.

■ P_{loss} & L_{index}

In the first case, three algorithms, MOPSO, MOAO, and MOIAO, are used to optimize the P_{loss} and L_{index} simultaneously. Each algorithm has been experimented with 30 times independently and the best result is selected from them for comparative analysis. Fig. 32 shows the Pareto fronts obtained by the three algorithms. The Pareto front distribution of MOIAO more closely resembles the true Pareto front than the other two algorithms. The optimal compromise results among the three algorithms along with the corresponding control variables are given in TABLE VIII. By comparing the data, the P_{loss} obtained by the MIAO is 5.1373 MW and the L_{index} is 0.1319. Its optimization results account for better than the MOPSO and MOAO in all aspects, and the P_{loss} is better than the results obtained by the MOIPSO in the literature [29].

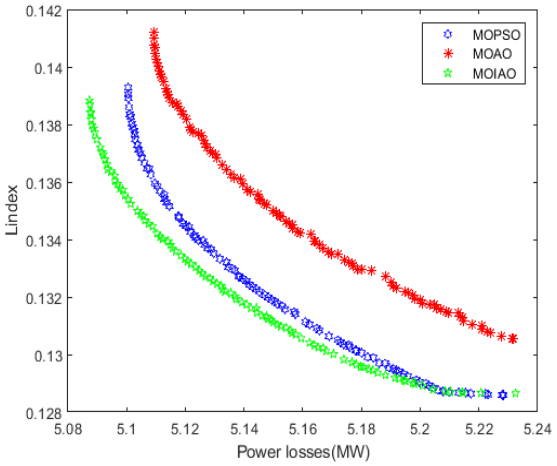

Fig. 32. Pareto fronts obtained by the three algorithms

■ P_{loss} & V_d

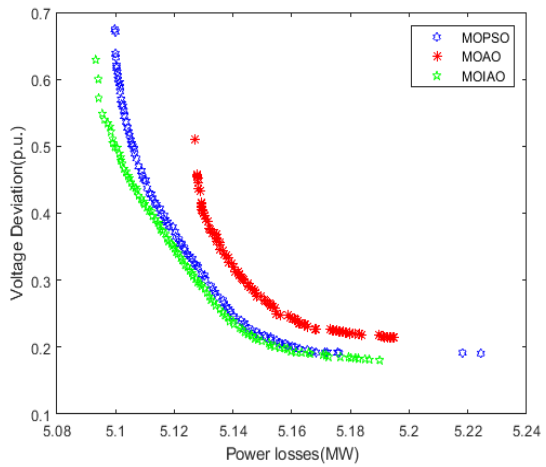

Fig. 33. Pareto fronts obtained by the three algorithms

In this case, the MOIAO is used to optimize the P_{loss} and V_d. In Fig. 33, it is evident that the Pareto frontier obtained by MOIAO is superior and the optimization results are relatively better compared to MOPSO and MOAO. The best compromise results of the three algorithms and the corresponding control variables are given in TABLE VIII. As shown in TABLE VIII, the best trade-off results obtained by the MOIAO for the optimization are: P_{loss} is 5.1388 MW and V_d is 0.2385 p.u., which is better than the other two algorithms and the GBICA in the literature [30], further proving the validity of the proposed method.

TABLE XVI
OPTIMIZATION OF THE BEST COMPROMISE SOLUTION AND CONTROL VARIABLES OBTAINED

Control variable	MOPSO	MOAO	MOIAO	CDQS-EICA[36]
V_{g1}(p.u.)	1.1000	0.9534	0.9500	1.0237
V_{g2}	1.0083	0.9577	0.9500	1.0159
V_{g5}	1.1000	0.9529	1.1000	0.9956
V_{g8}	1.1000	0.9553	1.1000	1.0299
V_{g11}	1.0985	0.9536	1.1000	1.0611
V_{g13}	1.1000	0.9590	1.1000	1.0817
$T_{6\text{-}9}$	1.0863	0.9534	0.9500	1.0703
$T_{6\text{-}10}$	0.9000	0.9577	0.9500	0.9529
$T_{4\text{-}12}$	1.1000	0.9529	1.1000	1.0961
$T_{28\text{-}27}$	0.9000	0.9553	1.1000	0.9000
Q_{c10}(p.u.)	0.0500	1.0452	1.0804	0.0161
Q_{c12}	0.0500	1.0053	0.9001	0.0041
Q_{c15}	0.0482	1.0887	1.0731	0.0000
Q_{c17}	0.0000	0.9018	0.9002	0.0171
Q_{c20}	0.0500	0.0188	0.0402	0.0438
Q_{c21}	0.0000	0.0179	0.0100	0.0113
Q_{c23}	0.0000	0.0500	0.0374	0.0370
Q_{c24}	0.0435	0.0421	0.0000	0.0107
Q_{c29}	0.0500	0.0287	0.0500	0.0290
V_d(p.u.)	0.4331	0.3986	**0.3929**	0.4374
L_{index}	0.1341	0.1359	**0.1348**	0.1337

■ V_d & L_{index}

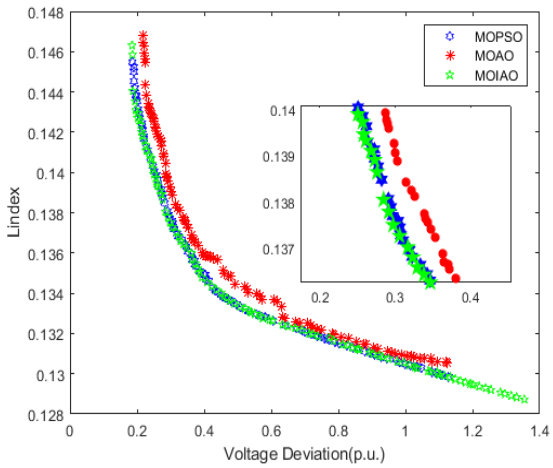

Fig. 34. Pareto fronts obtained by the three algorithms

In the third case, the Pareto fronts obtained by the three algorithms are shown in Fig. 34 for the simultaneous optimization of the V_d and L_{index}. It shows that the Pareto fronts obtained by both the MOPSO and the MOAO are very close to the Pareto front obtained by the MOIAO, but the MOIAO is more competitive in the distribution and uniformity of the Pareto fronts. To further verify the validity of the MOIAO, the optimization results obtained by the three

algorithms are analyzed. As shown in TABLE XVI, although the best compromise solution obtained by the MOIAO is slightly higher than the MOPSO and the CDQS-EICA in the literature [36] in terms of voltage stability index, the voltage deviation is much lower than their results. Compared to the best compromise solution obtained by the original MOAO again, the MOIAO is more dominant. It reinforces that the proposed MOIAO has the potential in solving ORPD problems.

D. IEEE57-bus Test System

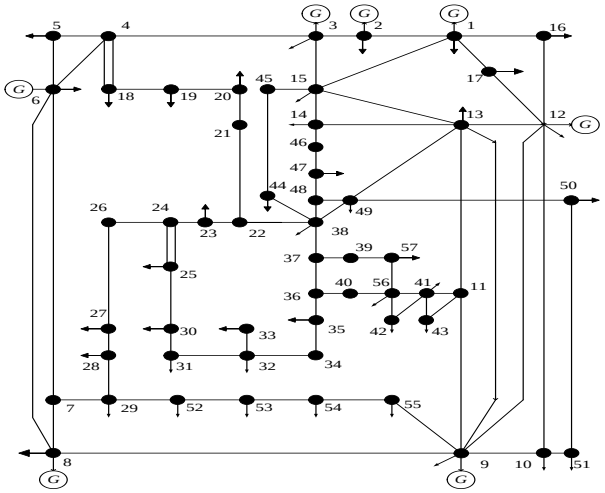

Fig. 35. Structure diagram of IEEE57-bus

TABLE XVII
LIMITS OF REACTIVE POWER OF GENERATORS IN IEEE57-BUS TEST SYSTEM

Bus number	$Q_{gi,min}$ (MVAr)	$Q_{gi,max}$ (MVAr)
1	-140	200
2	-17	130
3	-10	120
6	-8	55
8	-170	200
9	-3	70
12	-150	240

Fig. 35 shows the internal structure of the IEEE 57-bus system. TABLE XVII gives the important parameter limitations of the system.

1) P_{loss}

In the first case, IAO is applied to the P_{loss} optimization problem of the IEEE57-bus test system, and the results calculated by IAO are compared and analyzed with the classical GSA, PSO, and standard AO. The distribution plots of the optimization results of the four algorithms and the average convergence curves of 30 independent experiments are given in Fig. 26 and Fig. 27, respectively, which can be visualized that IAO has better distribution results and convergence. The best P_{loss} optimization values obtained by each algorithm and the corresponding control variable schemes are given in TABLE IX. The best P_{loss} result obtained by IAO is 22.2123 MW, which is 0.2962 MW, 0.8348 MW, and 0.6654 MW less than that of GSA, PSO, and standard AO, respectively. The validity of IAO in solving the reactive power optimization scheduling problem is further demonstrated. TABLE XVIII shows the results obtained by different methods proposed by previous researchers, it can be concluded that the method proposed in this paper is competitive.

TABLE XVIII
COMPARISON WITH LITERATURE RESULTS

Method	P_{loss}(MW)	V_d(p.u.)
IAO	**22.2123**	**0.6513**
ABC[15]	24.1025	-
ICA[16]	-	0.7952
GSA-CSS[18]	22.6991	0.6629
IGSA-CSS[18]	22.2718	-
SPSO[37]	24.4304	-
BBO[38]	24.5440	-
OGSA[39]	23.4300	-

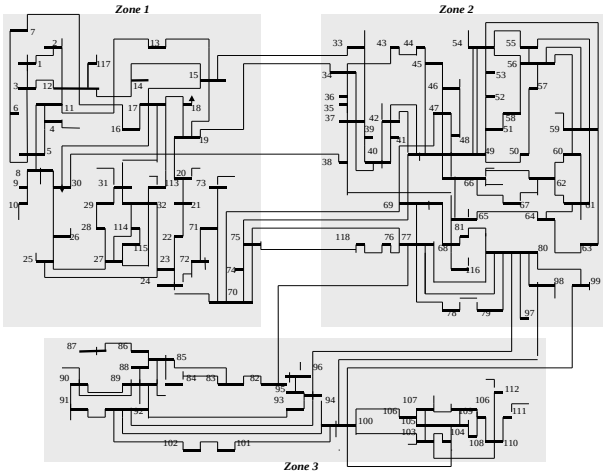

Fig. 36. Structure diagram of IEEE118-bus

2) V_d

In this case, Fig. 28 and Fig. 29 show better optimization results for V_d obtained by IAO. It can be seen from TABLE IX that IAO reduces the amount of V_d of the IEEE57-bus test system to 0.6513. Compared with the best optimization results of the other three algorithms and the algorithms in TABLE XVIII from previous years of literature, IAO obtains a better solution than the other methods.

E. IEEE118-bus Test System

Compared to the above test system, the IEEE118-bus test system is much larger. Fig. 36 shows the internal structure of the IEEE 118-bus system, with specific data referenced in the literature [40].

1) P_{loss}

To further verify the optimization capability of the improved method in large systems, it is applied to the IEEE 118-bus test system for simulation experiments. The distribution plots of the optimization results of the three algorithms and the average convergence curves of 30 independent experiments are given in Fig. 30 and Fig. 31. It can be intuitively seen that IAO converges better and the obtained experimental results are more uniformly distributed. The optimal value of active power loss optimization and the corresponding control variable scheme obtained by each algorithm are given in TABLE X. The optimal value obtained by IAO is 115.0060 MW, which is 10.6917 MW and 1.0542 MW less than GSA and standard AO, respectively, which further proves the high efficiency of IAO.

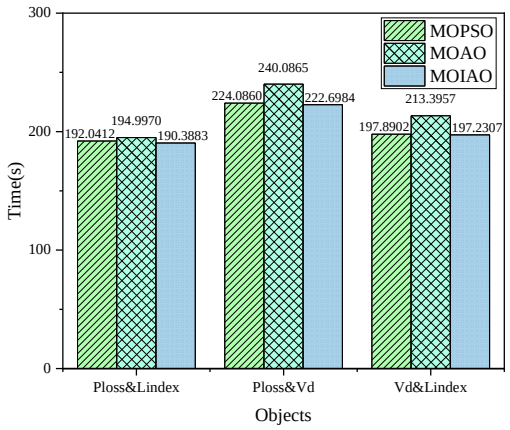

Fig. 37. CPU runtime

V. Conclusion

This paper presents IAO and successfully applied to the ORPD problem for nonlinear and multi-pole optimization problems considering both equality and inequality constraints. The performance of AO and IAO was simulated separately by different test functions and the test results showed that IAO performed better than AO. Moreover, three objective functions are considered, which are P_{loss}, V_d, and L_{index}. The proposed method performs SOORPD in four test systems of different sizes and performs MOORPD in IEEE30-bus test system. To verify the validity and reliability of IAO, the results were obtained and compared with the results in classical algorithms and historical literature. Results of the simulations have shown that the proposed method yields more competitive results and that the proposed improvement strategy is necessary for the studied test system. As can be seen from Fig. 37, IAO is superior in terms of computing time. Therefore, IAO has a great advantage in solving the ORPD problem with theoretical and practical value. It is believed that the proposed IAO is a promising candidate for the ORPD problem.

References

[1] O. Akdag, "A improved archimedes optimization algorithm for multi/single-objective optimal power flow," *Electric Power Systems Research*, vol. 206, article. 107796, 2022.

[2] Y. Liu, D. ćetenović, H. Li, E. Gryazina and V. Terzija, "An optimized multi-objective reactive power dispatch strategy based on improved genetic algorithm for wind power integrated systems," *International Journal of Electrical Power & Energy Systems*, vol. 136, article. 107764, 2022.

[3] Y. Wei, Y. Zhou, Q. Luo and W. Deng, "Optimal reactive power dispatch using an improved slime mould algorithm," *Energy Reports*, vol. 7, pp. 8742-8759, 2021.

[4] K. Nuaekaew, P. Artrit, N. Pholdee and S. Bureerat, "Optimal reactive power dispatch problem using a two-archive multi-objective grey wolf optimizer," *Expert Systems with Applications*, vol. 87, pp. 79-89, 2017.

[5] M. Nasouri Gilvaei, H. Jafari, M. Jabbari Ghadi and L. Li, "A novel hybrid optimization approach for reactive power dispatch problem considering voltage stability index," *Engineering Applications of Artificial Intelligence*, vol. 96, article. 103963, 2020.

[6] L. Lian, "Reactive power optimization based on adaptive multi-objective optimization artificial immune algorithm," *Ain Shams Engineering Journal*, vol. 13, no. 5, article. 101677, 2022.

[7] J. A. Momoh, S. X. Guo, E. C. Ogbuobiri and R. Adapa, "The quadratic interior point method solving power system optimization problems," *IEEE Transactions on Power Systems*, vol. 9, no. 3, pp. 1327-1336, 1994.

[8] T. Ding, S. Liu, W. Yuan, Z. Bie and B. Zeng, "A Two-Stage robust reactive power optimization considering uncertain wind power integration in active distribution networks," IEEE Transactions on Sustainable Energy, vol. 7, no. 1, pp. 301-311, 2016.

[9] M. A. M. Shaheen, H. M. Hasanien and A. Alkuhayli, "A novel hybrid GWO-PSO optimization technique for optimal reactive power dispatch problem solution," Ain Shams Engineering Journal, vol. 12, no. 1, pp. 621-630, 2021.

[10] J. Qian, P. Wang, C. Pu and G. Chen, "Joint application of multi-object beetle antennae search algorithm and BAS-BP fuel cost forecast network on optimal active power dispatch problems," Knowledge-Based Systems, vol. 226, article. 107149, 2021.

[11] G. Chen, J. Qian, Z. Zhang and S. Li, "Application of modified pigeon-inspired optimization algorithm and constraint-objective sorting rule on multi-objective optimal power flow problem," Applied Soft Computing, vol. 92, article. 106321, 2020.

[12] B. Ji, X. Yuan and Y. Yuan, "Modified NSGA-II for solving continuous berth allocation problem: Using multiobjective Constraint-Handling strategy," *IEEE Transactions on Cybernetics*, vol. 47, no. 9, pp. 2885-2895, 2017.

[13] H. T. Kahraman, M. Akbel and S. Duman, "Optimization of optimal power flow problem using Multi-Objective manta ray foraging optimizer," Applied Soft Computing, vol. 116, article. 108334, 2022.

[14] M. Ettappan, V. Vimala, S. Ramesh and V. T. Kesavan, "Optimal reactive power dispatch for real power loss minimization and voltage stability enhancement using Artificial Bee Colony Algorithm," *Microprocessors and Microsystems*, vol. 76, article. 103085, 2020.

[15] K. B. O. Medani, S. Sayah and A. Bekrar, "Whale optimization algorithm based optimal reactive power dispatch: A case study of the Algerian power system," Electric Power Systems Research, vol. 163, pp. 696-705, 2018.

[16] M. Mehdinejad, B. Mohammadi-Ivatloo, R. Dadashzadeh-Bonab and K. Zare, "Solution of optimal reactive power dispatch of power systems using hybrid particle swarm optimization and imperialist competitive algorithms," International Journal of Electrical Power & Energy Systems, vol. 83, pp. 104-116, 2016.

[17] A. H. Khazali and M. Kalantar, "Optimal reactive power dispatch based on harmony search algorithm," *International Journal of Electrical Power & Energy Systems*, vol. 33, no. 3, pp. 684-692, 2011.

[18] G. Chen, L. Liu, Z. Zhang and S. Huang, "Optimal reactive power dispatch by improved GSA-based algorithm with the novel strategies to handle constraints," *Applied Soft Computing*, vol. 50, pp. 58-70, 2017.

[19] Y. Li, Y. Wang and B. Li, "A hybrid artificial bee colony assisted differential evolution algorithm for optimal reactive power flow," *International Journal of Electrical Power & Energy Systems*, vol. 52, pp. 25-33, 2013.

[20] P. Subbaraj and P. N. Rajnarayanan, "Optimal reactive power dispatch using self-adaptive real coded genetic algorithm," *Electric Power Systems Research*, vol. 79, no. 2, pp. 374-381, 2009.

[21] H. Xiong, H. Cheng and H. Li, "Optimal reactive power flow incorporating static voltage stability based on multi-objective adaptive immune algorithm," *Energy Conversion and Management*, vol. 49, no. 5, pp. 1175-1181, 2008.

[22] W. Zhang and Y. Liu, "Multi-objective reactive power and voltage control based on fuzzy optimization strategy and fuzzy adaptive particle swarm," *International Journal of Electrical Power & Energy Systems*, vol. 30, no. 9, pp. 525-532, 2008.

[23] C. Dai, W. Chen, Y. Zhu and X. Zhang, "Reactive power dispatch considering voltage stability with seeker optimization algorithm," *Electric Power Systems Research*, vol. 79, no. 10, pp. 1462-1471, 2009.

[24] C. Huang and Y. Huang, "Combined differential evolution algorithm and ant system for optimal reactive power dispatch," *Energy Procedia*, vol. 14, pp. 1238-1243, 2012.

[25] A. A. A. E. Ela, M. A. Abido and S. R. Spea, "Differential evolution algorithm for optimal reactive power dispatch," *Electric Power Systems Research*, vol. 81, no. 2, pp. 458-464, 2011.

[26] S. Wang, H. Jia, L. Abualigah, Q. Liu and R. Zheng, "An improved hybrid aquila optimizer and harris hawks algorithm for solving industrial engineering optimization problems," *Processes*, vol. 9, no. 9, article. 1551, 2021.

[27] M. Abd Elaziz, A. Dahou, N. A. Alsaleh, A. H. Elsheikh and A. I. Saba *et al.*, "Boosting COVID-19 image classification using MobileNetV3 and aquila optimizer algorithm," *Entropy*, vol. 23, no. 11, article. 1383, 2021.

[28] L. Abualigah, D. Yousri, M. Abd Elaziz, A. A. Ewees and M. A. A. Al-Qaness *et al.*, "Aquila Optimizer: A novel meta-heuristic optimization algorithm," *Computers & Industrial Engineering*, vol. 157, article. 107250, 2021.

[29] G. Chen, L. Liu, P. Song and Y. Du, "Chaotic improved PSO-based

multi-objective optimization for minimization of power losses and L index in power systems," *Energy Conversion and Management*, vol. 86, pp. 548-560, 2014.
[30] M. Ghasemi, S. Ghavidel, M. M. Ghanbarian and M. Gitizadeh, "Multi-objective optimal electric power planning in the power system using Gaussian bare-bones imperialist competitive algorithm," *Information Sciences*, vol. 294, pp. 286-304, 2015.
[31] G. Chen, L. Liu and S. Huang, "Enhanced GSA-Based optimization for minimization of power losses in power system," *Mathematical Problems in Engineering*, vol. 2015, pp. 1-13, 2015.
[32] M. Ghasemi, M. M. Ghanbarian, S. Ghavidel, S. Rahmani and E. Mahboubi Moghaddam, "Modified teaching learning algorithm and double differential evolution algorithm for optimal reactive power dispatch problem: A comparative study," *Information Sciences*, vol. 278, pp. 231-249, 2014.
[33] M. Varadarajan and K. S. Swarup, "Differential evolution approach for optimal reactive power dispatch," *Applied Soft Computing*, vol. 8, no. 4, pp. 1549-1561, 2008.
[34] Z. Sahli, A. Hamouda, A. Bekrar and D. Trentesaux, "Reactive power dispatch optimization with voltage profile improvement using an efficient hybrid algorithm," *Energies*, vol. 11, no. 8, article. 2134, 2018.
[35] M. Tuba and N. Bacanin, "Improved seeker optimization algorithm hybridized with firefly algorithm for constrained optimization problems," *Neurocomputing*, vol. 143, pp. 197-207, 2014.
[36] G. Chen, J. Cao, Z. Zhang and Z. Sun, "Application of imperialist competitive algorithm with its enhanced approaches for multi-objective optimal reactive power dispatch problem," *Engineering Letters*, vol. 27, no. 3, pp. 579-592, 2019.
[37] C. Dai, W. Chen, Y. Zhu and X. Zhang, "Seeker optimization algorithm for optimal reactive power dispatch," *IEEE Transactions on Power Systems*, vol. 24, no. 3, pp. 1218-1231, 2009.
[38] A. Bhattacharya and P. K. Chattopadhyay, "Biogeography-Based Optimization for solution of Optimal Power Flow problem," in *ECTI-CON2010: The 2010 ECTI International Conference on Electrical Engineering/Electronics, Computer, Telecommunications and Information Technology*, Chiang Mai, Thailand, 2010, pp. 435-439.
[39] B. Shaw, V. Mukherjee and S. P. Ghoshal, "Solution of reactive power dispatch of power systems by an opposition-based gravitational search algorithm," *International Journal of Electrical Power & Energy Systems*, vol. 55, pp. 29-40, 2014.
[40] A. Rajan and T. Malakar, "Optimal reactive power dispatch using hybrid Nelder–Mead simplex based firefly algorithm," *International Journal of Electrical Power & Energy Systems*, vol. 66, pp. 9-24, 2015.